β-(*Z*) Selectivity Control by Cyclometalated Rhodium(III)-Triazolylidene Homogeneous and Heterogeneous Terminal Alkyne Hydrosilylation Catalysts

Beatriz Sánchez-Page,[a] Julen Munarriz,[b,c] M. Victoria Jiménez,[a] Jesús J. Pérez-Torrente,[a*] Javier Blasco,[d] Gloria Subias,[d] Vincenzo Passarelli,[e] and Patricia Álvarez[f]*

[a] Departamento de Química Inorgánica, Instituto de Síntesis Química y Catálisis Homogénea-ISQCH, Universidad de Zaragoza-C.S.I.C., 50009-Zaragoza, Spain. [b] Department of Chemistry & Biochemistry, University of California, Los Angeles (UCLA), Los Angeles, California 90095, United States. [c] Departamento de Química Física and Instituto de Biocomputación y Física de Sistemas Complejos (BIFI), Universidad de Zaragoza, Facultad de Ciencias, C/ Pedro Cerbuna 12, 50009, Zaragoza, Spain. [d] Instituto de Ciencia de Materiales de Aragón-ICMA, Departamento de Física de la Materia Condensada, CSIC-Universidad de Zaragoza, 50009 Zaragoza, Spain. [e] Centro Universitario de la Defensa, Ctra. Huesca s/n, ES-50090 Zaragoza, Spain. [f] Instituto de Ciencia y Tecnología del Carbono, INCAR, CSIC, P.O. Box, 73, 33080-Oviedo, Spain.

CORRESPONDING AUTHOR'S EMAIL: vjimenez@unizar.es, perez@unizar.es

KEYWORDS: graphene, covalent functionalization, N-heterocyclic carbenes, rhodium, hydrosilylation, reaction mechanism.

ABSTRACT

The cyclometalated Rh(III)-NHC compounds [Cp*RhI(C,C')-Triaz] (Triaz = 1,4-diphenyl-3-methyl-1,2,3-triazol-5-ylidene) and [Cp*RhI(C,C')-Im] (Im = 1-phenyl-3-methyl-imidazol-2-ylidene) are efficient catalysts for the hydrosilylation of terminal alkynes with complete regio- and stereoselectivity towards the thermodynamically less stable β-(*Z*)-vinylsilane isomer at room temperature in chloroform or acetone. Catalyst [Cp*RhI(C,C')-Triaz] shows a superior catalytic performance in terms of activity and has been applied to the hydrosilylation of a range of linear 1-alkynes and phenylacetylene derivatives with diverse hydrosilanes, including $HSiMePh_2$, $HSiMe_2Ph$, $HSiEt_3$ and the bulkier heptamethylhydrotrisiloxane (HMTS), to afford the corresponding β-(*Z*)-vinylsilanes in quantitative yields. The graphene-based hybrid material **TRGO-Triaz-Rh(III)**, featuring cyclometalated [Cp*RhI(C,C')-Triaz] (Triaz = 1,4-diphenyl-3-methyl-1,2,3-triazol-5-ylidene) rhodium(III) complexes covalently immobilized through the triazolylidene linker, has been prepared by metalation of the trimethylsilyl-protected 3-methyl-4-phenyl-1,2,3-triazolium iodide functionalized graphene oxide material, **TRGO-Triaz**, with $[Cp^*RhCl_2]_2$ using sodium *tert*-butoxide as base. The coordination sphere of the supported rhodium(III) complexes has been determined by means of XPS and extended X-ray absorption fine structure (EXAFS) spectroscopy, showing the replacement of the iodido ligand by O-functionalities on the carbon wall. In sharp contrast with the homogeneous catalyst, the heterogeneous hybrid catalyst **TRGO-Triaz-Rh(III)** is not active at room temperature although it shows an excellent catalytic performance at 60 ºC. In addition, the hybrid catalyst **TRGO-Triaz-Rh(III)** has shown an excellent recyclability allowing at least six catalytic runs in the hydrosilylation of oct-1-yne with $HSiMePh_2$ in acetone with complete selectivity to the β-(*Z*)-vinylsilane product. The reaction mechanism for the molecular catalyst [Cp*RhI(C,C')-Triaz] has been explored by means of DFT calculations, pointing to a metal–ligand bifunctional mechanism involving reversible cyclometalation that is competitive with a non-cooperative pathway. The

proposed mechanism entails the Rh–C_{Ar} assisted hydrosilane activation to afford a reactive Rh-silyl intermediate that leads to a (*E*)-silylvinylene intermediate after alkyne insertion and a metallacyclopropene-driven isomerization. The release of the β-(*Z*)-vinylsilane product can occur by a reversible cyclometalation mechanism involving σ-CAM with the C_{Ar}–H bond or, alternatively, the Si–H bond of an external hydrosilane. The energy barrier for the latter is 1.2 kcal·mol^{-1} lower than that of the C_{Ar}–H bond, which results in a small energy span difference that makes both pathways competitive under catalytic conditions.

INTRODUCTION

Catalysis is a key enabling technology for developing feasible solutions towards a sustainable chemical production.[1] In this context, the hydrosilylation of carbon-carbon multiple bonds is one of the most remarkable methods for the construction of Si–C bonds. In particular, the hydrosilylation of alkynes provides a straightforward and atom-economical access to vinylsilanes, which are useful intermediates in organic synthesis,[2] such as coupling partners in Hiyama cross coupling reactions,[3] or industrial reagents to synthesize cross-linked silicone polymers.[4] Despite major advances over the last years, the developing of transition-metal hydrosilylation catalysts for the control of the regio- and stereo-selectivity along the H–Si addition process is still a major challenge.

The hydrosilylation of terminal alkynes can afford three possible vinylsilane isomers, namely, the linear β-(*Z*) and β-(*E*) isomers resulting from the *syn*- and *trans*-anti-Markovnikov addition, respectively; and the branched α-vinylsilanes from the Markovnikov addition. Besides, the formation of silylalkyne derivatives, resulting from the competitive dehydrogenative silylation process, is occasionally observed for some catalytic systems (Scheme 1).[5] Although the β-(*E*)-vinylsilane formation generally occurs with high selectivity,[6] the selective synthesis of α-[7] and β-(*Z*)-isomers[8] is more challenging. Furthermore, the isomerization of β-(*Z*)-vinylsilanes to

thermodynamically more stable β-(*E*)-vinylsilanes under the typical conditions of transition-metal-catalyzed reactions constitutes an additional difficulty that hinders the development of β-(*Z*)-selective catalysts.[5,9] So far, a number of β-(*Z*)-selective noble-metal-based catalysts bearing Rh,[10] Ir[11] and Ru,[12] have been developed. However, many of them show either low reactivity or substrate-dependent selectivity, and usually produce a mixture of vinylsilane isomers. In addition, a few earth-abundant transition-metal based catalytic systems, such as Co,[13] Fe[14] and Mn,[15] have been recently reported to afford similar outcomes. A selection of β(*Z*)-stereoselective catalysts for terminal alkyne hydrosilylation is shown in Chart 1. However, these examples are still scarce, and therefore, the development of much more efficient catalysts to access the less thermodynamic stable β-(*Z*)-vinylsilane derivatives with wider applicability remains necessary.

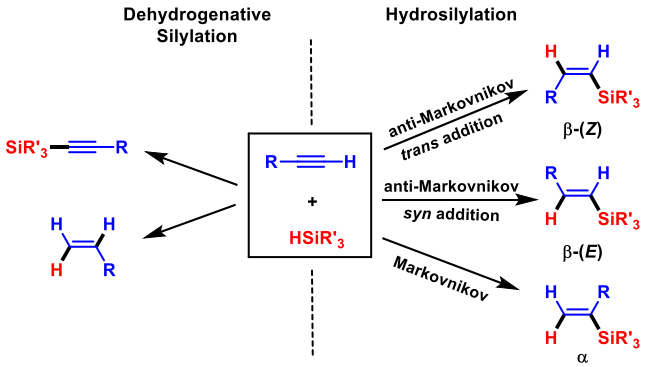

Scheme 1. Possible products for the hydrosilylation of terminal alkynes.

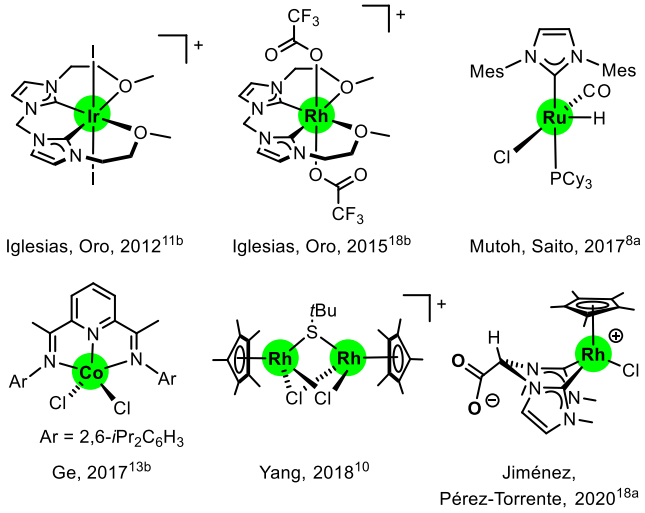

Chart 1. Leading catalysts for β(*Z*) stereoselective hydrosilylation of terminal alkynes.

Ligand design and mechanistic understanding are pivotal for the rational development of more efficient hydrosilylation catalysts. N-heterocyclic carbenes (NHCs) have been consolidated as powerful ligands for boosting catalytic activity owing to their strong coordination ability and tunable character, which enables the control of the steric and electronic properties at the metal center.[16] In this regard, considerable attention has been paid to the development of alkyne hydrosilylation rhodium catalysts based on functionalized NHC[6a,6c,17] and bis-NHC[7d,11b,18] ligands exhibiting different degrees of selectivity and efficiency. In particular, 1,2,3-triazolylidene (Triaz) ligands have emerged as a versatile subclass of NHCs with increased σ-donor properties, compared to classical Arduengo-type imidazol-2-ylidene ligands, and an electronic flexibility because of their mesoionic character derived from 1,3-disubstitution of the heterocyclic ring.[19,20] These properties make them powerful tools for catalyst design, and have found application in a range of catalytic transformations including cross coupling, olefin metathesis, water oxidation and the hydrosilylation of carbonyl compounds.[21] We have recently reported the efficiency of [RhI(cod)(Triaz)] (Triaz = 1,4-diphenyl-3-methyl-1,2,3-triazol-5-ylidene) as a catalyst for the hydrosilylation of a range of terminal and internal alkynes with good β-(*Z*) and *syn* selectivities, respectively, which constitutes the first example of a triazolylidene-based catalyst for this transformation.[22] Furthermore, we have set up a strategy for the immobilization of Rh(I)-triazolylidene complexes by making use of a bottom-up approach involving a stepwise solid phase synthesis of the corresponding triazolium fragments through the epoxy functionalities on thermally reduced graphene oxides (TRGO). This hybrid catalyst efficiently catalyzed the hydrosilylation of alkynes, showing the same good selectivity as the related [RhI(cod)(Triaz)] homogeneous catalyst. Noticeably, the good recyclability of the hybrid catalyst demonstrates the strength of the C–N covalent bond of the triazolylidene linker to the graphitic wall under hydrosilylation conditions. In this context, it is worth mentioning that a rather limited number of heterogenized rhodium hydrosilylation catalysts have been previously described in the literature.[23,24] To the best of our

knowledge, there are only two examples of Rh(I)-NHC catalysts covalently supported on carbonaceous materials, one of which showed moderate catalytic activity in the hydrosilylation of internal alkynes.[25] On the other hand, pyrene-tagged rhodium NHC complexes anchored onto reduced graphene oxide were found to be only moderately active for the hydrosilylation of terminal alkynes, and exhibited very limited recyclability.[26]

Keeping in mind the above results, we foresee the potential of cyclometalated rhodium(III) complexes, such as [Cp*RhI(C,C')-Triaz] or [Cp*RhI(C,C')-Im)] (Im = 1-phenyl-3-methyl-imidazolylide), as alkyne hydrosilylation catalysts. The combination of a supporting Cp* ligand with a strong donor NHC moiety engaged in a five-membered metalacycle, resulting from the ortho metalation of the phenyl substituent, provide a stable structural framework with possible application in hydrofunctionalization reactions. In particular, the Rh-C_{Ar} bond is a reactive site that could participate in the pre-catalyst activation by reaction with the hydrosilane[27] or the alkyne,[11a] thus affording reactive hydrosilylation intermediates.[28] Interestingly, reversible cyclometalation has been proposed as a possible metal-ligand bifunctional mechanism in catalysis.[29] In fact, computational studies have shown that the cooperativity of a cyclometalated metal-ligand fragment could be operative in the catalytic dehydrogenation of ammonia-borane and formic acid,[30] as well as in dehydrogenative silylation or transfer hydrogenation catalytic reactions.[31]

Herein, we report on the synthesis and characterization of a graphene-based hybrid catalyst featuring [Cp*RhI(C,C')-Triaz] complexes covalently immobilized through the triazolylidene linker as well as its application as heterogeneous catalyst for the hydrosilylation of a range of terminal alkynes with diverse hydrosilanes. In addition, we have carried out recyclability studies and a comparative study of its catalytic activity with that of related [Cp*RhI(C,C')-NHC] homogeneous catalysts. Moreover, the reaction mechanism for the molecular catalyst has been investigated by theoretical calculations at the Density Functional Theory (DFT) level. On the basis

of such calculations a metal-ligand bifunctional mechanism involving reversible cyclometalation could be feasible.

RESULTS AND DISCUSSION

Synthesis and Characterization of N-heterocyclic carbene Rhodium(III) complexes [Cp*RhI(C,C')-Triaz] (1) and [Cp*RhI(C,C')-Im] (2). Cyclometalated Rh(III)-NHC compounds **1** and **2** were prepared by reaction of the corresponding azolium salts, 1,4-diphenyl-3-methyl-1,2,3-triazolium iodide and 1-phenyl-3-methyl-imidazolium iodide, with half equivalent of the dimer compound $[Cp^*RhCl_2]_2$ in the presence of sodium tert-butoxide (Scheme 2).

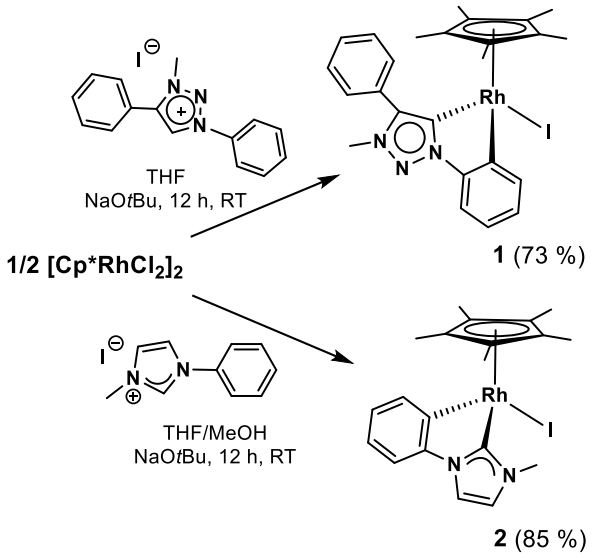

Scheme 2. Synthesis of cyclometalated complexes [Cp*RhI(C,C')-NHC] (NHC = Triaz, **1**; Im, **2**).

The formation of **1** proceeds through the mixed-halogen intermediate species [Cp*RhICl(Triaz)], which was observed when the reaction was conducted in the presence of 1 equivalent of NaO*t*Bu (see Supporting Information). It is worth noting that the related chlorido compound [Cp*RhCl(C,C)-Triaz] had previously been prepared by transmetalation of the triazolylidene silver compound to $[Cp^*RhCl_2]_2$ without any base.[32] However, regarding the covalent immobilization of this type of complexes on solid supports, the use of NaO*t*Bu is much more convenient as it avoids the use of a silver salt as well as the problems associated to the removal of the insoluble AgCl

byproduct. Compound **1** was obtained as an orange solid in 73% yield and fully characterized by elemental analysis, HRMS and NMR spectroscopy (see the Supporting Information).

The selective C–H activation of the N-bound phenyl group proposed for **1** was unambiguously confirmed by an X-ray diffraction analysis on a single crystal of the complex. The crystal structure of **1** shows a pseudo-tetrahedral environment at the metal centre (Figure 1a) similar to that already reported for the iridium-chlorido analogues.[32] The reduced bite angle of the cyclometalated triazolylidene ligand [C(1)-Rh-C(7) 78.6(3)º] distorts the coordination of both the C(1)-N(2)-N(3)-N(4)-C(5) and C(6)-C(7)-C(8)-C(9)-C(10)-C(11) rings, bringing about notable yaw angles ψ,[33] namely 13.7º and 5.5º, respectively. On the other hand, reduced pitch angles are observed [C(6)-C(7)-C(8)-C(9)-C(10)-C(11), pitch, θ 1.8º; C(1)-N(2)-N(3)-N(4)-C(5) pitch, θ 0.1º]. Furthermore, the steric release as well as the C(17)-H(17)···I contact (Figure 1a, C(17)-H(17) 0.95 Å, H(17)···I 3.04 Å, C(17)···I 3.954(6) Å, C(17)-H(17)-I 162º) should be responsible for the dihedral angle C(1)-C(5)-C(12)-C(17) of 41.6(1.1)º.

The cyclometalated iodido complex [Cp*RhI(C,C')-Im] (**2**) had already been prepared by Choudhury *et al*.[34] using NaOAc as base instead of NaO*t*Bu. Although the crystal structure of **2** was also reported, the poor quality of that determination, carried out at 293 K, *e.g.* R_1 = 0.1211 [$I>2\sigma(I)$], wR_2 = 0.4370 (all data), prompted us to perform a significantly more accurate study at 100 K. Both at 100 K and 293 K, the space group was $P2_1/c$, with slightly different unit cells. The ORTEP view of the crystal structure of **2** and a selection of bond lengths and angles are given in Figure 1b. It is worth mentioning that, due to the small bite angle of the phenyl-imidazolylidene metalated ligand [C(1)-Rh-C(12) 77.96(12)º], both the imidazolylidene moiety and the metalated phenyl ring deviate from the ideal arrangement at Rh-C(1) and Rh-C(12) bonds, respectively. In particular, they render the following pitch and yaw angles: C(7)-C(8)-C(9)-C(10)-C(11)-C(12), pitch, θ 7.4, yaw, ψ 6.8; C(1)-N(2)-C(3)-C(4)-N(5), pitch, θ 0.7º, yaw, ψ 10.5º.[33]

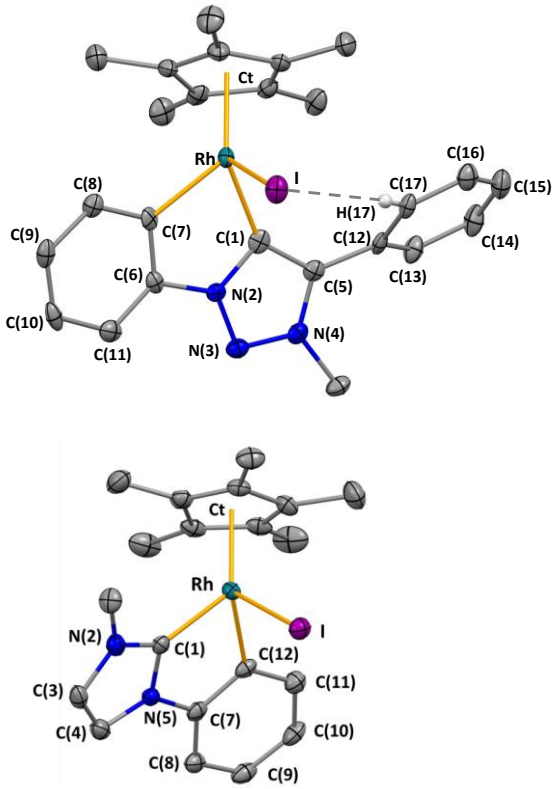

Figure 1. ORTEP views of [Cp*RhI(C,C')-NHC] with the thermal ellipsoids at 50 % probability. Most hydrogen atoms are omitted for clarity. Selected bond lengths (Å) and angles (º): a) **1**: C(1)-Rh 2.005(6), C(7)-Rh 2.048(7), Rh-I 2.6630(7), Rh-Ct 1.8577(5), C(1)-Rh-C(7) 78.6(3), C(1)-Rh-I 89.65(16), C(7)-Rh-I 88.89(17), Ct-Rh-C(7) 130.06(18), Ct-Rh-I 123.38(2), Ct-Rh-C(1) 131.47(18). b) **2**: C(1)-Rh 2.000(3), C(12)-Rh 2.049(3), Rh-I 2.6847(3), Rh-Ct 1.8702(2), C(1)-Rh-C(12) 77.96(12), C(1)-Rh-I 91.82(8), C(12)-Rh-I 95.47(8), Ct-Rh-C(1) 130.26(8), Ct-Rh-I 123.121(12), Ct-Rh-C(12) 125.56(8), C(1)-Rh-C(12) 77.96(12). Ct, centroid of the C_5 ring of the Cp* moiety.

Hydrosilylation of 1-alkynes catalyzed by [Cp*RhI(C,C')-NHC]. Compounds [Cp*RhI(C,C')-Triaz] (**1**) and [Cp*RhI(C,C')-Im] (**2**) were tested as catalyst precursors for the hydrosilylation of a range of aliphatic and aromatic terminal alkynes, including oct-1-yne, phenylacetylene derivatives and 3,3-dimethyl-but-1-yne; using $HSiMePh_2$, $HSiMe_2Ph$, and $HSiEt_3$ as hydrosilanes (see Table 1). The reactions were performed in $CDCl_3$ or acetone-d_6, at 25 or 60 ºC, with standard

catalyst loads of 1 mol % and were routinely monitored by ^{1}H NMR spectroscopy using anisole as internal standard.

Noteworthy, both catalysts are effective for the hydrosilylation of oct-1-yne with $HSiMe_2Ph$, affording full conversion and complete selectivity for the less thermodynamically stable β-(*Z*)-vinylsilane isomer using either acetone-d_6 or $CDCl_3$ as solvent. However, catalyst **1**, bearing the cyclometalated triazolylidene ligand, is more active than **2**. In fact, **1** catalyzes the hydrosilylation of oct-1-yne at room temperature either in chloroform or acetone, and significantly longer reaction times are needed for **2** (Table 1, entries 1-4). To our delight, the frequently observed catalyzed isomerization of β-(*Z*)-vinylsilane to the more thermodynamically stable β-(*E*)-vinylsilane isomer once the alkyne substrate has been completely exhausted is not observed here.[22,35] Further, the hydrosilylation reactions of oct-1-yne with less reactive hydrosilanes such as $HSiMePh_2$ or even $HSiEt_3$ proceed efficiently with both catalysts, affording complete selectivity for the β-(*Z*)-vinylsilane isomer (Table 1, entries 5-11). In general, hydrosilylation reactions with catalyst **1** are faster in acetone-d_6 than in $CDCl_3$ at room temperature, although the reaction speeds up significantly in $CDCl_3$ at 60 ^{o}C (entries 5 and 6).

The excellent catalytic performance of **1** in acetone-d_6 prompted us to study the substrate scope with this catalyst. Full conversion to the β-(*Z*)-vinylsilane product was attained in the hydrosilylation of phenylacetylene with $HSiMe_2Ph$ or $HSiEt_3$ in acetone-d_6 in about 20 min (entries 13 and 14). In contrast, the related Rh(I) catalyst [RhI(cod)Triaz] exhibited moderate catalytic activity and poor selectivity for the hydrosilylation of phenylacetylene.[22] The hydrosilylation of phenylacetylene derivatives having either an electron-donating (-OMe) or electron-withdrawing (-CF_3) substituent at the para position with $HSiMe_2Ph$ is slightly slower, especially for the latter, although complete selectivity to the β-(*Z*)-vinylsilane products was achieved with both substrates (entries 15 and 16).

The hydrosilylation of cyclohexylacetylene, a secondary alkyl substituted alkyne, with $HSiMe_2Ph$ and $HSiEt_3$ in $CDCl_3$ or acetone-d_6 also proceeds efficiently at 25 ^oC to give the corresponding β-(*Z*)-vinylsilane products (entries 17 and 19). On the other hand, the hydrosilylation of a bulky aliphatic alkyne such as t-Bu-C≡CH is much slower, even at 60 ºC, and pretty unselective, affording 68% of the β-(*E*)-vinylsilane (Table 1, entry 20), which is in agreement with the observed trend for related Rh(I)-NHC catalysts.[17c,18] Gratifyingly, the hydrosilylation of oct-1-yne with the least reactive and bulkier heptamethylhydrotrisiloxane (HMTS) takes place slowly at 60 ºC with complete selectivity to the β-(*Z*)-vinylsilane product (Table 1, entry 21).

To our delight, the hydrosilylation reaction can be carried out on a preparative scale as has been demonstrated for the synthesis of (*Z*)-dimethyl(oct-1-en-1-yl)(phenyl)silane by three consecutive catalytic cycles using catalyst **1** (see Experimental Section).

Table 1. Hydrosilylation of 1-alkynes catalyzed by [Cp*RhI(C,C')-NHC] (NHC = Triaz, **1**; Im, **2**).[a,b]

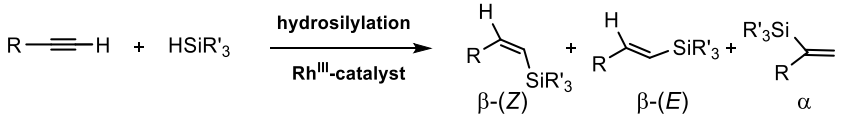

entry	1-alkyne / hydrosilane	solvent	T (ºC)	catalyst	t (min)	conv (%)	β-(*Z*) (%)	β-(*E*) (%)	α (%)
1	*n*-HexC≡CH/ $HSiMe_2Ph$	$CDCl_3$	25	**1**	20	98	99	-	-
2			25	**2**	360	99	99	-	-
3		acetone-d_6	25	**1**	15	98	99	-	-
4			25	**2**	110	99	99	-	-
5	*n*-HexC≡CH/ $HSiMePh_2$	$CDCl_3$	25	**1**	300	99	99	-	-
6			60	**1**	20	99	99	-	-
7			60	**2**	120	99	99	-	-
8		acetone-d_6	25	**1**	54	99	99	-	-
9			60	**2**	150	99	99	-	-
10	*n*-HexC≡CH/ $HSiEt_3$	$CDCl_3$	25	**1**	70	98	99	-	-
11		acetone-d_6	25	**1**	48	97	99	-	-
12	PhC≡CH/ $HSiMe_2Ph$	$CDCl_3$	25	**1**	20	99	99	-	-

13		acetone-d_6	25	**1**	18	98	99	-	-
14	PhC≡CH/HSiEt$_3$	acetone-d_6	25	**1**	22	99	99	-	-
15	MeOC$_6$H$_4$-C≡CH/ HSiMe$_2$Ph	acetone-d_6	25	**1**	50	97	99	-	-
16	CF$_3$C$_6$H$_4$-C≡CH/ HSiMe$_2$Ph	acetone-d_6	25	**1**	85	96	99	-	-
17	CyC≡CH/ HSiMe$_2$Ph	CDCl$_3$	25	**1**	45	99	99	-	-
18		acetone-d_6	25	**1**	40	99	99	-	-
19	CyC≡CH/HSiEt$_3$	acetone-d_6	25	**1**	20	99	99	-	-
20	*t*-BuC≡CH/ HSiMe$_2$Ph	acetone-d_6	60	**1**	240	98	24	68	8
21	*n*-Hex-C≡CH /HMTS	acetone-d_6	60	**1**	1000	98	99	-	-

a) Conversions and selectivities (%) were calculated by ^{1}H NMR using anisole as internal standard. b) Experiments were carried out in CDCl$_3$ or acetone-d_6 (0.5 mL) using a HSiR$_3$/alkyne/catalyst ratio of 100/100/1, [catalyst]$_o$ = 1 x 10^{-3} M.

We have studied the hydrosilylation of phenylacetylene with the hydrosilanes Ph$_2$SiH$_2$ and PhSiH$_3$ catalyzed by **1** at 60 °C in CDCl$_3$. Both reactions are unselective due to the formation of multi-addition products,[36] which is consistent with the high activity exhibited by catalyst **1**. Hydrosilylation of phenylacetylene with PhSiH$_3$ or Ph$_2$SiH$_2$ (1:1) afforded a mixture of mono- and di-alkenylsilane products with complete regioselectivity for the β-styryl derivatives, although the *Z* stereoselectivity is lost. Phenylacetylene reacted with PhSiH$_3$ (3:1 molar ratio, 4 h) to the give the tris-styrylsilane product (87%) as the *ZEE* (53%) and *EEE* (34%) stereoisomers. In contrast, the hydrosilylation of phenylacetylene with Ph$_2$SiH$_2$ (2:1) gave diphenyl((*Z*)-styryl)silane (47%) and diphenyl((*Z*)-styryl)((*E*)-styryl)silane (53%) in 40 min thereby suggesting that under these experimental conditions the first hydrosilylation proceeds with β-(*Z*) stereoselectivity (see Supporting Information).

Mechanistic insights on the hydrosilylation of 1-alkynes catalyzed by 1. In order to shed light on the mechanism of the hydrosilylation of terminal alkynes catalyzed by **1**, and understand its outstanding activity and selectivity, we performed a complete theoretical study. In particular, we

applied DFT at the B3LYP-D3BJ/def2-TZVP//def2-SVP (PCM, acetone) level of theory (see the Experimental Section for more details). We selected $HSiMe_2Ph$ and phenylacetylene as hydrosilane and alkyne models, respectively. The active catalyst (complex **1**) was considered in its totality, without including geometrical simplifications, as it bears reactive and bulky ligands that are likely to have a relevant effect in the reaction pathways.[37,38] For the sake of a clear understanding, the reaction intermediates and transition states are referred to by capital letters starting by **A** (which corresponds to the catalyst, **1**). Notice that we have set the energy reference at **D'**, as this species is the most likely starting point for successive catalytic cycles. The lowest-in-energy reaction pathway is shown in Figure 2, while other discarded alternatives are provided in Figure 3.

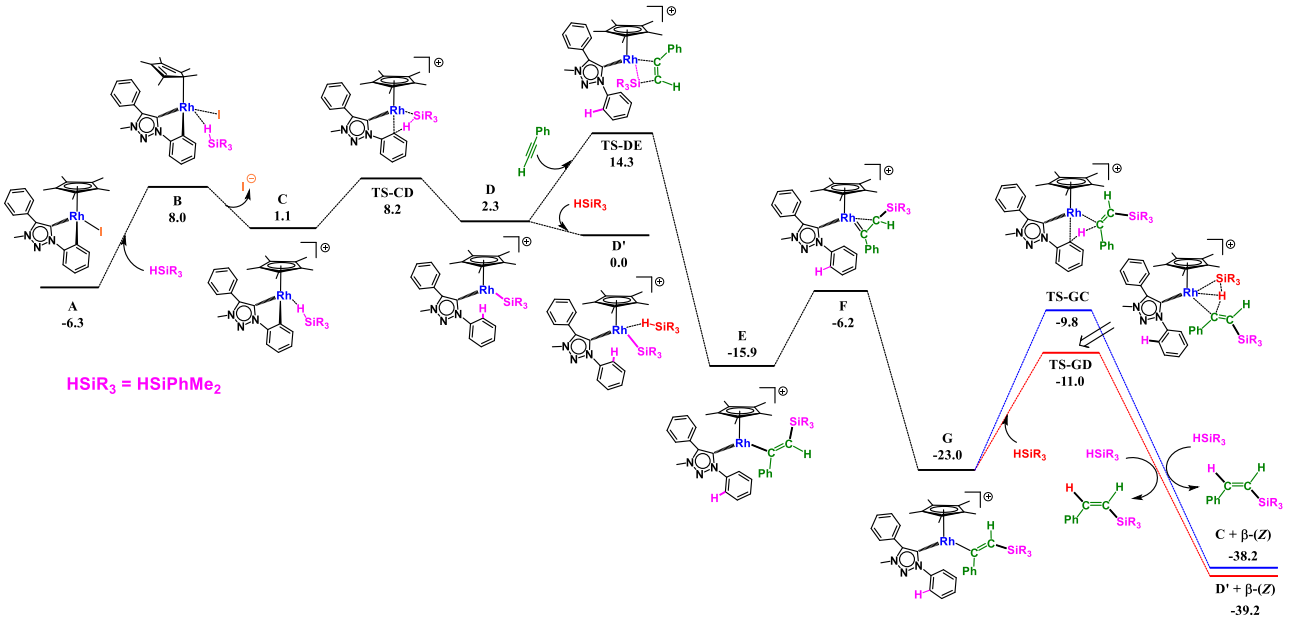

Figure 2. DFT calculated Gibbs energy reaction profile (in kcal·mol^{-1} relative to **D'** and isolated molecules) for the hydrosilylation of phenylacetylene with $HSiMe_2Ph$ catalyzed by [Cp*RhI(C,C')-Triaz] (**1**).

The first step consists on the ligand exchange between the iodido ligand and a hydrosilane molecule. This happens through intermediate **B**, which is 14.3 kcal·mol^{-1} less stable than **A**, and yields intermediate **C**, which is 7.4 kcal·mol^{-1} higher in energy than **A**. Notice that the aforementioned process is facilitated by the coordination flexibility of the Cp* ligand, which

changes its coordination mode form η^5 to η^1,[39,40] as we previously reported for structurally related catalysts.[37] Then, the hydrosilane H–Si bond is activated by means of a σ-complex assisted metathesis (σ-CAM) mechanism involving the H–Si and Rh–C_{Ar} bond, thus forming new Rh–Si and C–H bons.[41,42] This step proceeds *via* **TS-CD** (see Figure S34 in the Supporting Information), and requires to surmount an energy barrier of 14.5 kcal·mol^{-1} (with respect to **A**, feasible under the working conditions), leading to the silyl intermediate **D**, whose relative energy is 1.2 kcal·mol^{-1} higher than that of **C**. We note that we also explored the classical inner-sphere mechanisms that involve the hydrosilane oxidative addition to the metal center,[43] but we could not find any stable intermediate. In fact, the oxidative addition on Rh(III) species **A** (and **C**) would lead to a Rh(V) intermediate, which, with very few exceptions,[44] has been extensively reported to be unstable.

As **D** bears a coordination vacancy, both the hydrosilane and the alkyne could occupy it. The coordination of the hydrosilane would lead to **D'**, 2.3 kcal·mol^{-1} more stable that **D**; however, this pathway could not further evolve as the oxidative addition of the hydrosilane into the Rh(III) center would lead to a Rh(V) intermediate. Also notice that the significant steric repulsions within the complex hinder the hydrosilane coordination, thereby resulting in a stabilization energy of only 2.3 kcal·mol^{-1}. The ligand exchange between the hydrosilane and the alkyne leads to **D''**, 2.4 kcal·mol^{-1} less stable than **D'**, which has not been included in Figure 2 for simplicity. Nonetheless, this step is necessary for the alkyne insertion into the Rh–Si bond, which takes place *via* **TS-DE** (see Figure S34 in the Supporting Information) and yields the (*Z*)-silylvinylene intermediate **E**, with a relative energy of -15.9 kcal·mol^{-1} with respect to **D'**. The process requires to overcome an energy barrier of 20.6 kcal·mol^{-1} (with respect to **A)** for the first catalytic cycle, and 14.3 kcal·mol^{-1} (with respect to **D'**), for successive cycles (see below).

Intermediate **E** may undertake three different processes, which are summarized in Figure 3. One possibility is a direct σ-CAM between the C_{Ar}–H and Rh–C bonds to directly yield the

β-(*E*)-vinylsilane product (via **TS-EC**, Figure 4a) and **C** (blue pathway). This process would require to overcome an energy barrier of 16.1 kcal·mol^{-1}, determined by the energy difference between **E** and the transition structure **TS-EC**. The second possibility would be σ-CAM with a newly coordinated hydrosilane, *i.e.* between the H–Si and the Rh–C bonds, to yield the β-(*E*)-vinylsilane product and **D**, by means of **TS-ED** (Figure 4b), as shown in the red pathway. This pathway would require to overcome an energy barrier of 23.8 kcal·mol^{-1} (the energy difference between **TS-ED** and **E**). Alternatively, **E** can isomerize to intermediate **G**, with a relative energy of -23.0 kcal·mol^{-1}, 7.0 kcal·mol^{-1} more stable than **E** (black pathway). This process may take place via a metallacyclopropene intermediate **F**, also named η^2-vinylsilane metal species,[45] with a relative energy of -6.2 kcal·mol^{-1} (9.7 kcal·mol^{-1} higher than **E**). Notice that the energetic profile of this process is significantly lower than that involving the direct β-(*E*)-vinylsilane formation (9.7 kcal·mol^{-1} *vs* 23.8 kcal·mol^{-1} and 16.1 kcal·mol^{-1}), and thus the isomerization pathway will be the preferred one. On balance, intermediate **F** leads to the isomerization of the (*Z*)-silylvinylene into the more stable (*E*)-silylvinylene intermediate. We associate the feasibility of the formation of the three-membered metallacycle intermediate to the presence of a coordination vacancy in the 16e$^-$ intermediate **E**, which facilitates the coordination of a second carbon atom to the metal center, thus forming intermediate **F**.

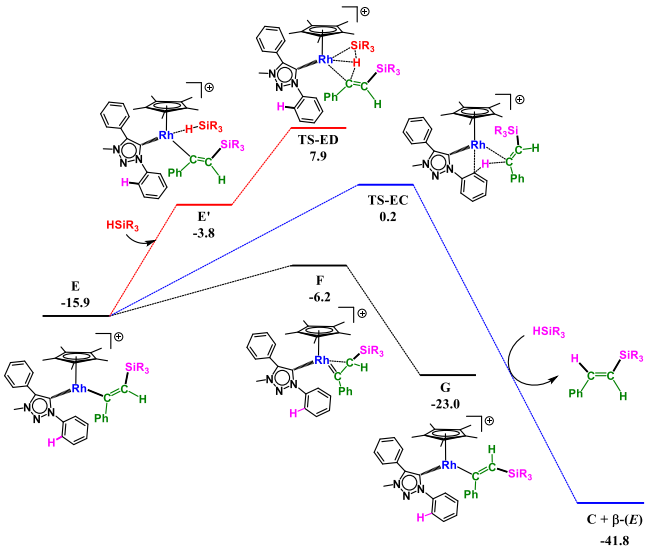

Figure 3. Possible reaction pathways to be undertaken for intermediate **E** (in kcal·mol^{-1} relative to **D'** and isolated molecules).

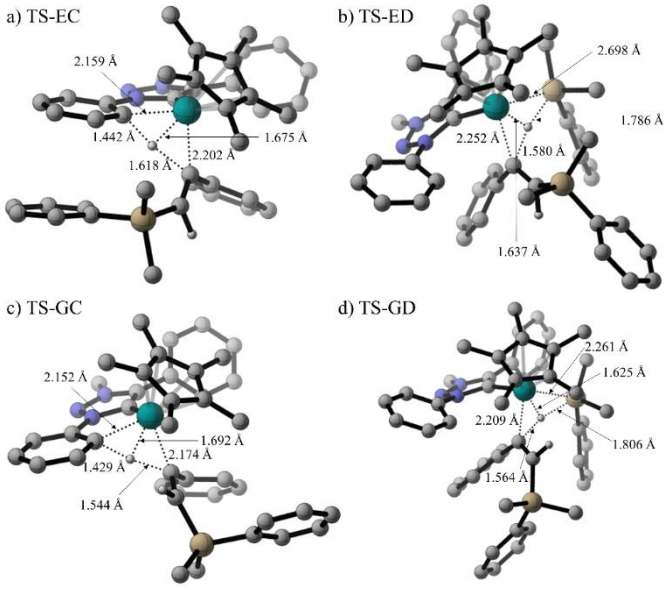

Figure 4. DFT-optimized structures and selected distances of: a) **TS-EC**, b) **TS-ED**, c) **TS-GC** and d) **TS-GD**. Notice that non-relevant hydrogen atoms have been omitted for clarity.

Finally, there would be two different possibilities for the generation of the β-(*Z*)-vinylsilane product from **G** by means of σ-CAM processes, which are analogous to those reported for the formation of the β-(*E*)-vinylsilane isomer (see Figure 2). The first one consists on the cyclometalation via σ-CAM between H–C_{Ar} and Rh–C bonds through **TS-GC** (Figure 4c), with an energy barrier of 13.2 kcal·mol^{-1} (dictated by the energy difference between **TS-GC** and **G**), which would regenerate intermediate **C** and yield the β-(*Z*)-vinylsilane (blue pathway in Figure 2). The second alternative (red pathway) involves the coordination of another hydrosilane molecule and the σ-CAM between the H–Si and the Rh–C bonds (via TS-GD, Figure 4d), with an energy barrier of 12.0 kcal·mol^{-1} (determined by the difference between **TS-GD** and **G**). This pathway leads to the β-(*Z*)-vinylsilane and intermediate **D'** (upon coordination of a hydrosilane in the coordination vacancy of **D**).

Remarkably, **TS-GD** is 1.2 kcal·mol^{-1} more stable than **TS-GC**, pointing towards the σ-CAM between the H–Si and the Rh–C bonds is preferred to the reversible cyclometalation; however, the very small energy difference between both pathways indicates that both will contribute to the overall reaction ensemble. It is also noticeable that the transition state for cyclometalation was 7.7 kcal·mol^{-1} more stable than the σ-CAM with the hydrosilane for the (*E*)-silylvinylene intermediate (**E**), while it is 1.2 kcal·mol^{-1} less favorable for the (*Z*)-silylvinylene intermediate (**G**). We attribute this feature to the higher steric hindrance in **E**, which disfavors the hydrosilane coordination (see Figure 4).

Overall, the process is very favorable from a thermodynamic point of view, with a Δ*G* of -39.2 kcal·mol^{-1} with respect to **D'** (and -32.9 kcal·mol^{-1} with respect to **A**) for the β-(*Z*)-vinylsilane product. We calculated the effective energy span (Δ*G*‡) for the cycle by means of the method proposed by Kozuch *et al.*[46] According to this framework, the first catalytic cycle features Δ*G*‡ of 20.6 kcal·mol^{-1}, which is determined by the energy difference between **TS-DE** (the alkyne insertion into the Rh–Si bond) and **A**. However, since the lowest-in-energy pathway leads to **D'**, we set the *zero* of energies in this point as it is the starting point for subsequent cycles. Thus, the energy span for the subsequent reaction cycles would be Δ*G*‡ = 12.0 kcal·mol^{-1}, which corresponds to the final σ-CAM between the H–Si hydrosilane bond and the Rh–C bond of the (*Z*)-silylvinylene (**G**).[47]

The proposed mechanism for the hydrosilylation of phenylacetylene with $HSiMe_2Ph$ catalyzed by [Cp*RhI(C,C')-Triaz] (**1**) on the basis of theoretical calculations is summarized in Scheme 3. The release of the β-(*Z*)-vinylsilane product from the (*E*)-silylvinylene intermediate can occur by a reversible cyclometalation mechanism involving σ-CAM with the C_{Ar}–H bond (outer catalytic cycle),[30a] or the Si–H bond of an external hydrosilane (inner catalytic cycle). Since the energy barrier for the σ-CAM pathway involving the Si–H bond is 1.2 kcal·mol^{-1} lower than that of the C–H bond, both pathways could be operative under the experimental reaction conditions.

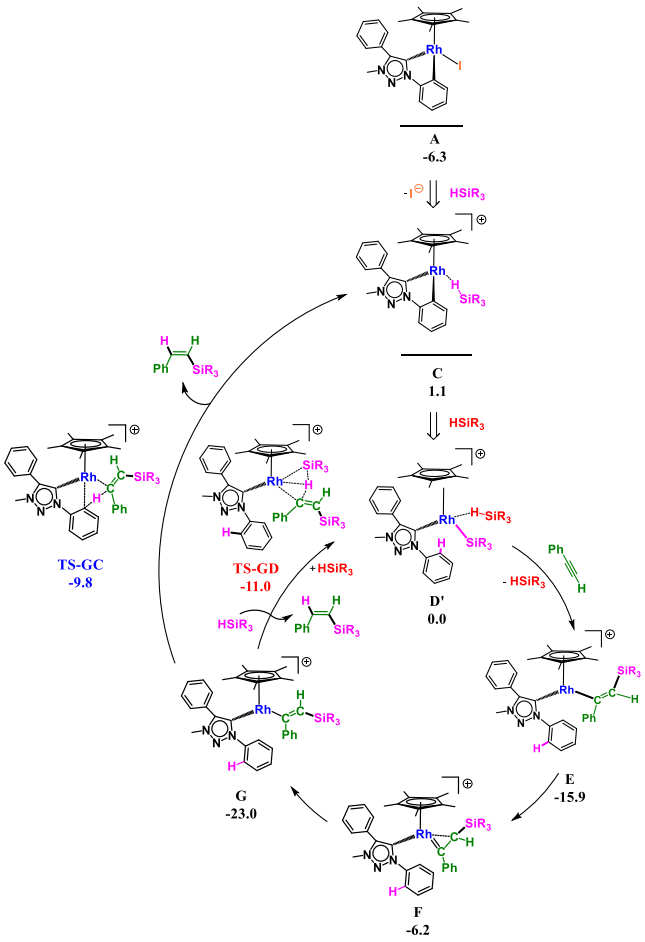

Scheme 3. Mechanistic proposal for the hydrosilylation of phenylacetylene with $HSiMe_2Ph$ catalyzed by [Cp*RhI(C,C')-Triaz] (**1**) made on the basis of DFT calculations.

In order to analyze in depth, the role of steric effects in the reaction mechanism, we recomputed the aforementioned reaction pathways for an alky-substituted NHC-Rh complex in which we have replaced the phenyl moiety in the NHC scaffold by a methyl group. For analogy with catalyst **1**, we called this one **1-Me**, which corresponds to intermediate **A-Me** in the theoretically-computed reaction pathways (see Figures S35 and S36 in the Supporting Information). The results showed that a similar reaction mechanism takes place when the bulkier phenyl group is substituted by a methyl one (Figures S35 and S36), with minor changes in the energy barriers, as a consequence of the lower steric hindrance of the Me group. Namely, the energy span for the alkyne insertion in the Rh–Si bond (determined by **TS-CD-Me** and **D'-Me** for the second catalytic cycle on) is 9.6 kcal·mol^{-1}, *i.e.* 4.7 kcal·mol^{-1} lower than that derived from the original catalyst (**1**). On the contrary,

the energy difference between the η^2-vinylsilane metal intermediate (**F-Me**) and the β(E)-vinylsilane formation by σ-CAM-driven orthometalation (**TS-EC-Me**) is 6.8 kcal·mol^{-1}, only 0.4 kcal·mol^{-1} higher than that of **1** (Figures 3 and S36); thus indicating that both catalysts will undertake the same isomerization process to yield the β(Z)-vinylsilane isomer. Probably, the most remarkable difference is that the energy splitting between the two possibilities for the release of the final product (energy difference between **TS-GD-Me** and **TS-GC-Me**, Figure S35) is significantly higher for **1-Me**, the σ-CAM between the H–Si hydrosilane bond and the Rh–C bond of G-Me being 5.6 kcal·mol^{-1} more favorable than the orthometalation, while it is only 1.2 kcal·mol^{-1} for **1**. As a consequence, we only expect the former process to take place. We attribute this difference to the lower steric hindrance in **1-Me**. As **TS-GD(-Me)** is more sterically impeded, the substitution of the phenyl moiety by a methyl one, relieves the steric repulsion, making this transition structure significantly lower in energy than that of **TS-GC(-Me)**, in which the steric repulsion effect is less important as its coordination sphere is less crowded (it misses the extra silane present in **TS-GD(-Me)**)

Synthesis and Characterization of Graphene-Based Rhodium(III)-Triazolylidene Hybrid Catalyst. The remarkable alkyne hydrosilylation performance of the cyclometalated [Cp*RhI(C,C')-Triaz] (**1**) compound prompted us to prepare a related graphene-oxide-supported Rh(III)-triazolylidene hybrid material. A 3-methyl-4-phenyl-1,2,3-triazolium iodide functionalized graphene oxide material having trimethylsilyl-protected hydroxy groups recently reported by us, **TRGO-Triaz**, has been used for this purpose (Scheme 4). According to our previous experience, the protection of all -OH groups in the triazolium functionalized material is required for the successful metalation that leads to triazolylidene rhodium complexes anchored to the carbon nanomaterial. In fact, the TMS-protected Rh(I)-triazolylidene (TMS = trimethylsilyl) hybrid material has shown excellent stability and good recyclability for alkyne hydrosilylation, thereby confirming the strength of the C–N covalent bond of the triazolylidene to the graphitic wall.[22]

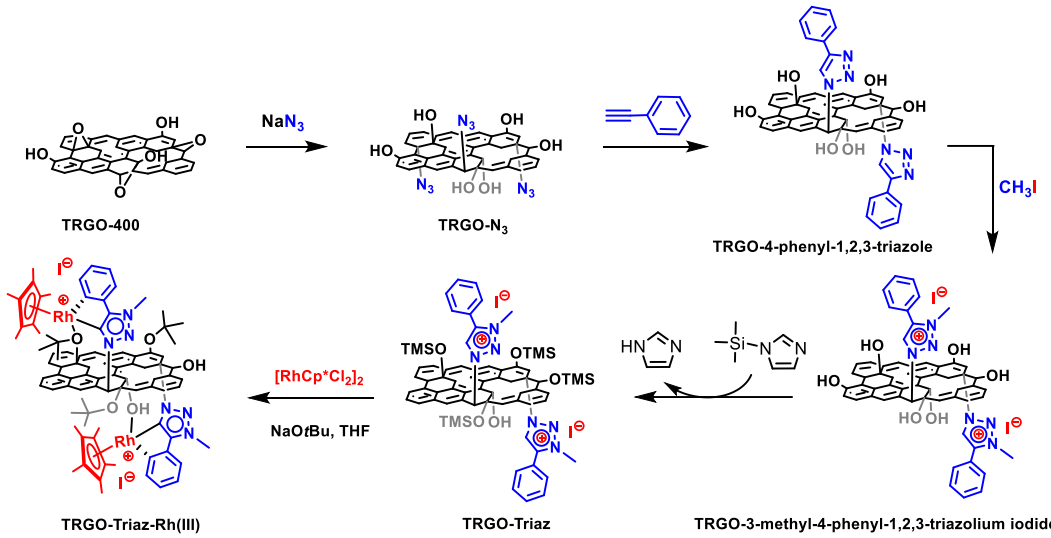

Scheme 4. Stepwise synthesis and structure of the graphene-based Rh(III)-triazolylidene hybrid catalyst **TRGO-Triaz-Rh(III)** (see the Supporting Information for details).

The graphene supported Rh(III)-triazolylidene hybrid material, **TRGO-Triaz-Rh(III)**, was prepared by reaction of **TRGO-Triaz** with $[Cp^*RhCl_2]_2$ in the presence of sodium *tert*-butoxide. The rhodium content of the new hybrid material, 5.7 wt.%, was determined by means of ICP-MS. HRTEM images (Figure 5a) and STEM-EDX mapping (Figures 5b, I-IV) of **TRGO-Triaz-Rh(III)** establish the homogeneous distribution of the rhodium atoms (black spots of size between 0.7-1.2 nm, Figure 5a) all along the graphene basal planes (Figure 5b, II).[22,48] Similarly, nitrogen and oxygen are also homogeneously distributed in the graphene material (Figure 5b, III-IV, respectively) although silicon was almost undetectable. A similar result was obtained by the analysis of this sample by XPS (see Supporting information, Table S1) confirming that the silicon content observed in the parent **TRGO-Triaz** material (5.3 %) have disappeared after rhodium anchoring. The presence of Rh(III) in **TRGO-Triaz-Rh(III)** was evidenced by the doublet signal in the high-resolution XPS Rh3d spectrum with an average separation between the maxima of ~4.6 eV and with the maximum of the 3d5/2 peak centered at ~310.1 eV (Figure S9, see Supporting Information).[49]

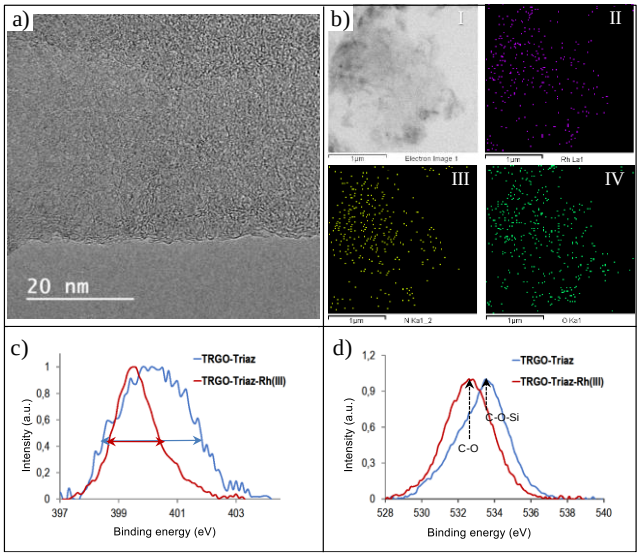

Figure 5. a) HRTEM, b) STEM (I) and EDX mapping images of Rh (II), N (III) and O (IV) for **TRGO-Triaz-Rh(III)**, and high resolution XPS spectra of c) N1s and d) O1s for **TRGO-Triaz** (blue curves) and **TRGO-Triaz-Rh(III)** (red curves).

On the other hand, the anchorage of rhodium to the triazolylidene moieties was evidenced by a change in the XPS N1s spectra (Figure 5c). Not only the maximum of the signal is shifted to lower binding energies (from 400.2 to 399.5 eV), but also a narrowing of the signal is observed with full widths at half maximum, FWHM, of 1.6 and 3.3 eV for **TRGO-Triaz-Rh(III)** and **TRGO-Triaz**, respectively. These effects were also observed in the in the XPS N1s spectra of the previously reported **TRGO-Triaz-Rh(I)** compared to that of **TRGO-Triaz**.[22] Surprisingly, when analyzing the high resolution XPS O1s spectra (Figure 5d), a shift in the maximum towards lower binding energies is also seen after rhodium anchoring. This significant fact is consistent with the elimination of the C–O–Si bonds involving the protective TMS groups, which is in accordance with the observed absence of Si in the hybrid material. Besides, the higher intensity at lower binding energies in that spectrum does not discard the formation of Rh–O bonds. Moreover, the deconvolution of the high resolution XPS C1s spectra confirms a substantial increase in the Csp^3 content after rhodium anchoring (from 15.5 % to 34.5% for **TRGO-Triaz** and **TRGO-Triaz-Rh(III)**, respectively; see Table S1 in the Supporting Information). All in all, the significant

increment in the Csp^3 content after rhodium anchoring seems to be related to the release of the TMS protecting groups from **TRGO-Triaz** as Me_3SiOH due to the protonation with the tert-butanol generated in the formation of the triazolylidene rhodium complex. As a consequence, tert-butoxy moieties are linked to the graphitic wall of **TRGO-Triaz-Rh(III)** as ether groups. The elimination of the TMS protective groups was also indirectly confirmed by XPS analysis of the **TRGO-Triaz'** material. Such system was obtained by treatment of **TRGO-Triaz** at the same experimental conditions as those used to prepare **TRGO-Triaz-Rh(III)** but in the absence of $[Cp^*RhCl_2]_2$, that is, with NaO*t*Bu in THF and additional washing with methanol. The resulting material **TRGO-Triaz'**, exhibits a negligible XPS Si content. Moreover, the same effect was observed when the material **TRGO-Triaz** was treated directly with *t*-BuOH. The XPS of this washed material **TRGO-Triaz''** confirms the lability of the protective groups under the experimental conditions.

In order to shed more light on the local structure of the Rh(III) atoms in the hybrid material **TRGO-Triaz-Rh(III)**, Extended X-ray Absorption Fine Structure (EXAFS) spectra at the Rh K edge were measured. EXAFS analysis was also related with that of the molecular complex [Cp*RhI(C,C')-Triaz] (**1**) and compared with those of the known [RhI(cod)Triaz] (cod = 1,5-cyclooctadiene) rhodium(I) molecular compound and the TMS-protected **TRGO-Triaz-Rh(I)** hybrid material.[22] Focusing on the properties of **TRGO-Triaz-Rh(III)** and **1**, their EXAFS spectra (EXAFS signals and the Fourier transforms (FT), see Figure S12, Supporting Information) clearly indicate different environments for the Rh(III) atoms in both samples. The FT allows us to determine a strong peak at a distance of about 1.65 Å (without phase shift correction) for **TRGO-Triaz-Rh(III)** that agrees with Rh–C or Rh–O interatomic distances. Contributions beyond this first coordination shell are weak, suggesting the lack of heavier atoms close to the Rh centers. On the other hand, the FTs of **1** show two peaks of similar intensity at distances of 1.65 and 2.40 Å. The first peak is less intense with respect to the previous samples, indicating either a smaller

coordination number or a greater disorder in the Rh–C (or O) coordination shell. The second distance is in agreement with a Rh–I interatomic distance, suggesting that the iodido ligand is in the first coordination shell for the molecular complexes, but not for the hybrid material. This behavior is similar to that previously observed for [RhI(cod)Triaz] and the TMS-protected **TRGO-Triaz-Rh(I)** hybrid material.[22]

The EXAFS fit was performed in the R-space between 1.1 and 3.1 Å for **TRGO-Triaz-Rh(III)** and between 1.1 and 3.9 Å for **1**. In order to have an appropriate model to analyse the spectrum of **1**, we have made use of the crystallographic data for this compound to calculate phases and amplitudes of the different paths, as indicated in the Experimental Section. Figure 6a shows the experimental spectrum and the best fit obtained for this sample. The analysis is in accordance with the crystallographic data and the Rh presents a piano stool geometry formed by the Cp* ligand, two shorter Rh–C distances which belong to the orthometalated N-phenyl group and to the carbene of the triazolylidene ligand, and a iodine atom for the last coordination position. Regarding the analysis of **TRGO-Triaz-Rh(III)**, it is clear that the previous model fails to account for the local environment of the Rh center, as no iodido is found in the first coordination shell. Following previous results on rhodium and iridium carbon supported materials,[22,48] we have replaced the I atom by an O in the Rh neighborhood. To our delight, the fit quickly converges, reaching the outcome shown in the Figure 6b. This result reveals that the iodine has been replaced by an oxygen in the Rh coordination sphere. The most likely possibility is that the oxygen belongs to one of the -OH or -O-*t*Bu groups on the carbon wall to complete the rhodium coordination, instead of the iodido, which is clearly not present in the immediate vicinity of Rh atoms in this hybrid material (see Figure 6c). The refined parameters of both fits are summarized in Table S3 in the Supporting Information.

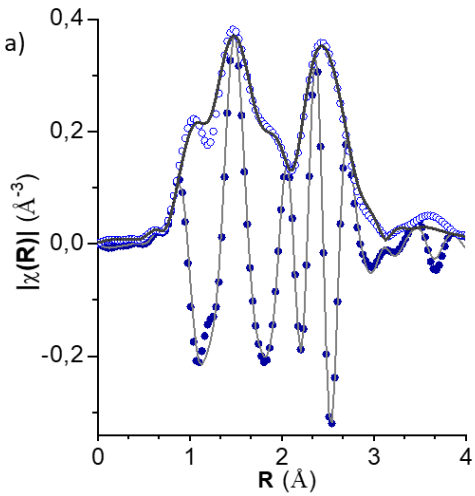

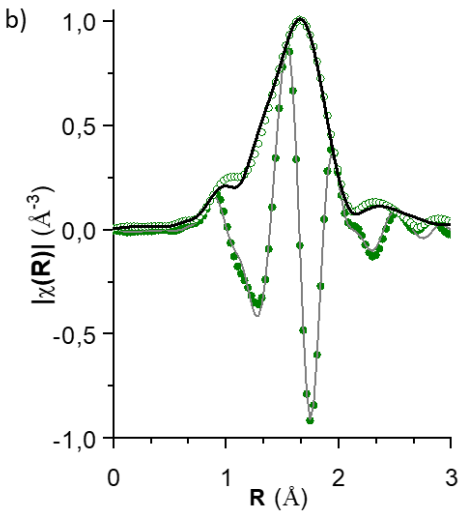

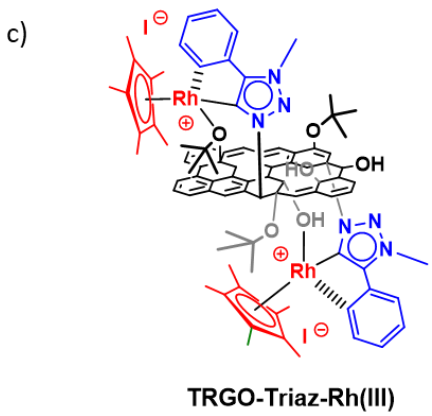

Figure 6. Best fits (lines) and experimental (circles) FTs curves (open for moduli and dark for the real parts) for: a) [Cp*RhI(C,C')-Triaz] (**1**) and b) **TRGO-Triaz-Rh(III)**, c) structural model for the hybrid **TRGO-Triaz-Rh(III)** material.

Catalytic activity in hydrosilylation of 1-alkynes and recycling of the hybrid catalyst TRGO-Triaz-Rh(III). The catalytic activity of the heterogeneous graphene-based catalyst **TRGO-Triaz-Rh(III)** in the hydrosilylation of terminal alkynes has been studied and compared with that of the molecular homogeneous catalyst [Cp*RhI(C,C')-Triaz] (**1**) (Table 2). The reactions were carried out in $CDCl_3$ or acetone-d_6 using a catalyst load of 1 mol% of Rh (calculated according to the rhodium content of 5.7 wt.% from ICP-MS) and monitored by ^{1}H NMR spectroscopy.

In contrast to **1**, **TRGO-Triaz-Rh(III)** showed no catalytic activity at room temperature neither in acetone-d_6 nor in $CDCl_3$. However, at 60 ºC, the hybrid catalyst is an effective catalyst for the hydrosilylation of oct-1-yne with hydrosilanes such as $HSiMe_2Ph$ or $HSiMePh_2$ affording full conversion and complete selectivity for the β-(*Z*)-vinylsilane isomer in less than 40 min in both solvents (entries 1-8). Remarkably, although the hydrosilylation of oct-1-yne with $HSiEt_3$ requires around 100 min it proceeds with excellent selectivity in both solvents (entries 9 and 10).

TRGO-Triaz-Rh(III) efficiently catalyzed the hydrosilylation of aromatic alkynes. Phenylacetylene was selectively transformed into the corresponding β-(*Z*)-vinylsilane product in acetone-d_6 at 60 ºC using $HSiMe_2Ph$ or $HSiEt_3$ in 30 and 240 min, respectively (entries 11 and 12). Interestingly, complete β-(*Z*) selectivity was attained in the hydrosilylation of phenylacetylene derivatives having electronically dissimilar substituents at the para position in acetone-d_6 at 60 °C (entries 13 and 14). These results contrast with the performance of the related Rh(I) hybrid catalyst **TRGO-Triaz-Rh(I)**, for which extensive phenylacetylene polymerization was observed.[50] As can be observed in the reaction profiles for the hydrosilylation of 4-R-C_6H_4-C≡CH derivatives (R = H, MeO and CF_3) with $HSiMe_2Ph$ (Figure 7), the presence of a -OMe electron-donating group resulted in a slightly increase in the catalytic activity compared to phenylacetylene. However, the hydrosilylation of the phenylacetylene derivative with an electron-withdrawing substituent such as CF_3 is much slower. According to the negative slope of the Hammett plot (ρ = -0.63 for TOF_{50}) a buildup of positive charge in the transition state of the reaction is occurring and consequently a rate

increase by electron-donor groups is observed due to resonance stabilization (see Figure S29 in the Supporting Information).[21b]

Table 2. Hydrosilylation of 1-alkynes catalyzed by the hybrid catalyst **TRGO-Triaz-Rh(III)**.[a,b]

entry	1-alkyne / hydrosilane	solvent	T (ºC)	t (min)	conv (%)	β-(*Z*) (%)	β-(*E*) (%)	α (%)
1	*n*-HexC≡CH/ $HSiMe_2Ph$	$CDCl_3$	25	30	0	0	-	-
2			60	30	99	99	-	-
3		acetone-d_6	25	30	0	0	-	-
4			60	30	99	99	-	-
5	*n*-HexC≡CH/ $HSiMePh_2$	$CDCl_3$	25	30	0	0	-	-
6			60	40	98	99	-	-
7		acetone-d_6	25	30	0	0	-	-
8			60	36	99	99	-	-
9	*n*-HexC≡CH/ $HSiEt_3$	$CDCl_3$	60	100	97	99	-	-
10		acetone-d_6	60	90	98	99	-	-
11	PhC≡CH/ $HSiMe_2Ph$	acetone-d_6	60	30	98	99	-	-
12	PhC≡CH/$HSiEt_3$	acetone-d_6	60	240	98	99	-	-
13	$MeOC_6H_4$-C≡CH/ $HSiMe_2Ph$	acetone-d_6	60	30	99	99	-	-
14	$CF_3C_6H_4$-C≡CH/ $HSiMe_2Ph$	acetone-d_6	60	76	98	99	-	-
15	*t*-BuC≡CH/ $HSiMe_2Ph$	acetone-d_6	60	300	97	25	66	9
16	*n*-HexC≡CH /HMTS	acetone-d_6	60	1100	99	99	-	-

a) Conversions and selectivities (%) were calculated by ^{1}H NMR spectroscopy using anisole as internal standard. b) Experiments were carried out in $CDCl_3$ or acetone-d_6 (0.5 mL) using a $HSiR_3$/alkyne/catalyst ratio of 100/100/1, 1 mol% of Rh calculated according to ICP-MS measurements.

As observed for the homogeneous catalyst **1**, the hydrosilylation of the bulky *t*-Bu-C≡CH with $HSiMe_2Ph$ by **TRGO-Triaz-Rh(III)** was unselective, affording a similar product distribution with β-(*E*)-vinylsilane as the major reaction outcome (entry 15). Notice that the hydrosilylation of oct-1-yne with heptamethylhydrotrisiloxane (HMTS) is β-(*Z*)-selective although, as for catalyst **1**, a much longer reaction time (18 h) is required (entry 16). Importantly, no β-(*Z*) to β-(*E*) vinylsilane

isomerization was observed in the catalyzed hydrosilylation of oct-1-yne with $HSiMe_2Ph$ neither with **TRGO-Triaz-Rh(III)** nor with **1**, even when heating during long reaction times.

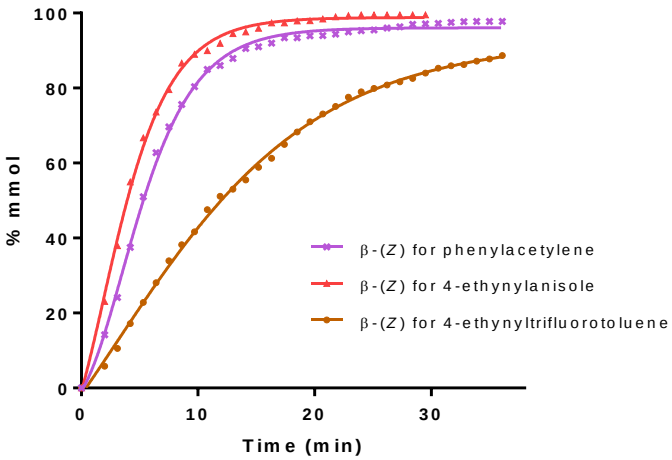

Figure 7. Reaction profile obtained from ^{1}H NMR data for the hydrosilylation of arylacetylenes derivatives 4-R-C_6H_4-C≡CH (R = H, purple; MeO, salmon; and CF_3, brown) with $HSiMe_2Ph$ (1:1), catalyzed by **TRGO-Triaz-Rh(III)** in acetone-d_6 (0.5 mL) at 60 °C with 1 mol% of Rh calculated according to ICP-MS measurements.

Catalyst recycling experiments with **TRGO-Triaz-Rh(III)** for the hydrosilylation of oct-1-yne with both $HSiMePh_2$ and $HSiMe_2Ph$ have been carried out in acetone-d_6 at 60 ºC using a catalyst load of 1 mol% of Rh. The recycling experiments (run n) were carried out by evaporating the solvent under vacuum, washing the residue with fresh n-hexane (3 x 1 mL) and then, adding a new load of hydrosilane/oct-1-yne/acetone-d_6 (Table 3). Remarkably, the recovered heterogeneous catalyst after the catalysis runs exhibited identical performance as the fresh catalyst after 5 consecutive cycles for both hydrosilanes. The recycling runs were performed under an argon atmosphere, except for the last run that was carried out on air (entries 6 and 12). The catalytic reactions were monitored by ^{1}H NMR, and showed very similar kinetic profiles in the successive recycling experiments, even for the last cycle. The recycled heterogeneous catalyst recovered after the successive catalysis runs, **TRGO-Triaz-Rh(III)-R**, was characterized by means of XPS.

Interestingly, the N1s and Rh3d spectra, accounting only for the supported organometallic moiety, are similar to that of the parent **TRGO-Triaz-Rh(III)**. This analysis confirms structural similarities for the metal centre before and after the catalytic cycles, which points towards similar oxidation states and the maintenance of the C–N moieties (see the Supporting Information). Finally, in order to control the stability of the immobilized rhodium(III) complex in the **TRGO-Triaz-Rh(III)** hybrid catalyst, the possible rhodium leaching along the catalytic runs was investigated. We did so by means of ICP-MS analysis of the filtrate and washings after each run in the hydrosilylation of oct-1-yne with $HSiMePh_2$ (Table 3, entries 1-6) to determine their Rh content. A 0.5 % loss of the initial Rh content was observed after the first run. This is consistent with the removal of physisorbed rhodium species, not eliminated by the standard material washing, but likely removed under the catalytic reaction conditions. Remarkably, no rhodium leaching was detected in the following runs (Figure 8) thereby confirming the stability of the graphene-based rhodium(III)-triazolylidene hybrid catalyst.

Table 3. Catalyst recycling experiments for the hydrosilylation of oct-1-yne catalyzed by the hybrid catalyst **TRGO-Triaz-Rh(III)**.[a,b]

entry	*n*-HexC≡CH /hydrosilane		t(min)	conv %	β-(*Z*) (%)
1	$HSiMePh_2$	Run 1	40	99	>99
2		Run 2	40	99	>99
3		Run 3	40	99	>99
4		Run 4	40	98	>99
5		Run 5	40	99	>99
6		Run 6[c]	40	98	>99
	$HSiMe_2Ph$	Run 1	30	99	>99
8		Run 2	30	99	>99
9		Run 3	30	98	>99
10		Run 4	30	98	>99
11		Run 5	30	98	>99
12		Run 6[c]	30	98	>99

a) Conversions and selectivities (%) were calculated by ^1H NMR using anisole as internal standard. b) Experiments were carried out in acetone-d_6 (0.5 mL) at 60 ºC, using a $HSiR_3$/oct-1-yne/catalyst ratio of 100/100/1, 1 mol% of Rh calculated according to the ICP measurements. c) Recycling experiment carried out on air.

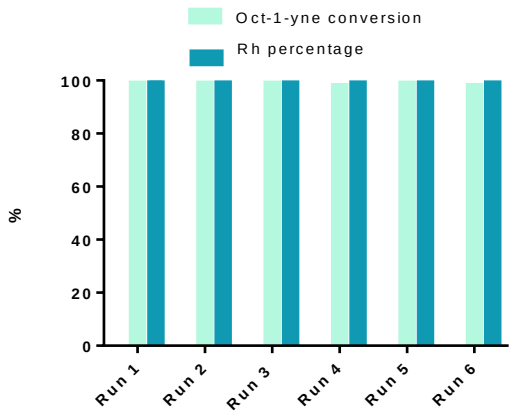

Figure 8. Recycling of **TRGO-Triaz-Rh(III)** in the hydrosilylation of oct-1-yne with $HSiMePh_2$ in acetone-d_6 for six catalytic runs (reaction time of 40 min). Oct-1-yne conversion and Rh percentage in the recycled material in base of the Rh content, analyzed by ICP-MS, of the filtrate and washings after each run.

CONCLUSIONS

The cyclometalated Rh(III)-NHC compound [Cp*RhI(C,C')-Triaz] (Triaz = 1,4-diphenyl-3-methyl-1,2,3-triazol-5-ylidene) is an efficient catalyst for the hydrosilylation of terminal alkynes with complete regio- and stereoselectivity towards the thermodynamically less stable β-(*Z*)-vinylsilane isomer at room temperature both in chloroform and acetone. Linear 1-alkynes, such as oct-1-yne, tert-butylacetylene and phenylacetylene derivatives undergo hydrosilylation with diverse hydrosilanes, including $HSiMePh_2$, $HSiMe_2Ph$, $HSiEt_3$ and the bulkier heptamethylhydrotrisiloxane (HMTS), to afford the corresponding β-(*Z*)-vinylsilanes in quantitative yields.

We have applied our strategy for the immobilization of Rh(I)-triazolylidene compounds on carbonaceous materials, which has demonstrated the strength of the C–N covalent bond of the triazolylidene linker to the graphitic wall under hydrosilylation conditions, to prepare a Rh(III)-triazolylidene hybrid catalyst. The graphene-based hybrid material featuring covalently immobilized cyclometalated [Cp*RhI(C,C')-Triaz] complexes through the triazolylidene linker,

TRGO-Triaz-Rh(III), has been prepared by metalation of the trimethylsilyl-protected 3-methyl-4-phenyl-1,2,3-triazolium iodide functionalized graphene oxide material, **TRGO-Triaz**, with $[Cp^*RhCl_2]_2$ using sodium *tert*-butoxide as base. The coordination sphere of the supported rhodium(III) complexes has been determined by means of XPS and extended X-ray absorption fine structure (EXAFS) spectroscopy showing the replacement of the iodido ligand by O-functionalities on the carbon wall. Furthermore, experimental studies in combination with XPS measurements evidence the elimination of the trimethylsilyl protective groups which are replaced by tert-butoxy moieties linked to the graphitic wall as ether groups. The heterogeneous **TRGO-Triaz-Rh(III)** hybrid catalyst is not active at room temperature although it shows an excellent catalytic performance in acetone at 60 ºC, comparable to that of the homogeneous catalyst [Cp*RhI(C,C')-Triaz], and excellent recyclability, as it has been reused in six consecutive cycles without loss of activity while maintaining the selectivity.

DFT studies on the reaction mechanism in the process involving the molecular catalyst [Cp*RhI(C,C')-Triaz] have shown two feasible (and competitive) mechanistic scenarios: i) a metal–ligand bifunctional mechanism involving reversible cyclometalation and, ii) a non-cooperative pathway. The proposed cooperative pathway entails the Rh–C_{Ar} assisted hydrosilane activation to afford a reactive Rh-silyl intermediate. Regioselective 2,1-alkyne insertion into the Rh-Si bond affords a (*Z*)-silylvinylene intermediate which is isomerized to the (*E*)-silylvinylene through a metallacyclopropene intermediate with the relief of steric strain between the Cp*Rh metal fragment and the adjacent silyl as the driving force of the process. Finally, the H-transfer from the flanking phenyl ring to the (*E*)-silylvinylene by means of a σ-CAM with the C_{Ar}–H bond leads to the β-(*Z*)-vinylsilane product restoring the Rh-C bond. However, the release of the β-(*Z*)-vinylsilane product from the (*E*)-silylvinylene intermediate can also occur by a mechanism involving σ-CAM with the Si–H bond of an external hydrosilane. It has been found that the energy barrier for the σ-CAM pathway involving the Si-H bond is only 1.2 kcal·mol^{-1} lower than that of

the C–H bond. As the turnover-determining transition state is determined by the energy barrier of the σ-CAM processes, the energy span difference between both mechanisms is also small and thus, both pathways are likely to be competent under catalytic conditions. For comparison, we also computed the reaction pathways for the catalysis resulting of the substitution of the phenyl substituent in **1** by a methyl group (**1-Me**). The calculations point towards the same reaction mechanism taking place with **1-Me**. However, in this case the energy barrier for the σ-CAM pathway involving the Si–H bond is 5.6 kcal·mol^{-1} lower than that of the C–H bond, so we expect that only the former alternative would take place.

EXPERIMENTAL

General Considerations. All reactions were carried out under under argon using Schlenk techniques. Solvents were distilled immediately prior to use from the appropriate drying agents or obtained from a Solvent Purification System (Innovative Technologies). The azolium salts, 1,4-diphenyl-3-methyl-1,2,3-triazolium iodide[51] and 1-phenyl-3-methyl-1,3-imidazolium iodide,[52] and the rhodium starting material $[Cp^*RhCl_2]_2$[53] were prepared according to the literature methods. The trimethylsilyl-protected, 3-methyl-4-phenyl-1,2,3-triazolium iodide functionalized graphene oxide material, **TRGO-Triaz**, was prepared from a thermally partially reduced graphene oxide by a three steps solid-phase procedure followed by the protection of the -OH groups by reaction with trimethylsilylimidazole (see Supporting Information).[22] All other reagents were commercially available and used as received.

Specific Equipment. Thermogravimetric analyses (TGA) were performed on a TA SDT 2960 analyzer. The procedure was as follows: 3 mg of sample was heated in the thermobalance to 1000 ºC at 10 ºC min^{-1} using a nitrogen:air flow (1:1) of 200 mL min^{-1}. High-resolution transmission electron microscopy (HRTEM) images were obtained using a JEOL JEM-2100F transmission electron microscope, equipped with a field-emission-gun (FEG) and operating at 200 kV. Elemental analyses were carried out on a Perkin-Ekmer 2400 Series-II CHNS/O micro-analyzer or

a LECO-CHNS-932 micro-analyser equipped with a LECO-VTF-900 furnace coupled to the micro-analyser.

X-ray photoemission spectroscopy (XPS) spectra were performed on a SPECS system operating under a pressure of 10^{-7} Pa with a Mg Kα X-ray source. The functional groups in the graphene-based materials were quantified by deconvolution of the corresponding high resolution XPS peaks using a peak analysis procedure that employs a combination of Gaussian and Lorentzian functions and a Shirley baseline.[54] The spectra did not require charge neutralization and were subsequently calibrated to the C1s line at 284.5 eV. The binding energy profiles for the C1s spectra were deconvoluted as follows: undamaged structures of Csp^2-hybridized carbons (284.5 eV), damaged structures or Csp^3-hybridized carbons (285.5 eV), C–OH groups (286.5 eV), O–C–O functional groups (287.7 eV) and C(O)OH groups at 288.7 eV. The O1s spectra were deconvoluted using the components C=O/COO (531.7 eV), C–O (533.5 eV) and C–O–Si (533.6 eV). For the N1s spectra, different components were used depending on the nature of the material analyzed and includes -N=N– (400.0 eV), –N– (401.1 eV) and $=N^+=$ (402.8 eV). The amount of rhodium in the hybrid catalysts was determined by means of Inductively Coupled Plasma Mass Spectrometry (ICP-MS) in an Agilent 7700x instrument.[55] Raman spectroscopy was performed on a Renishaw 2000 Confocal Raman Microprobe using a 514.5 nm argon ion laser. Spectra were recorded from 750 to 3500 cm^{-1}.

X-ray absorption spectroscopy (XAS) measurements at the Rh K edge were recorded at room temperature on the CLAESS beamline[56] at the ALBA synchrotron (Cerdanyola del Vallès, Spain). The storage ring was operating at 3 GeV with a current of 120 mA. The EXAFS spectra were measured with a Si (311) double crystal monochromator and harmonic rejection was carried out with a Pt strip in the vertical collimator. Estimated energy resolution, $\Delta E/E$, at the Rh K edge was better than 10^{-4}. The XAS spectra were measured in the transmission mode using pellets diluted with cellulose, if necessary, in order to optimize the absorption jump. The XAS spectra were

normalized to unity edge jump and the k weighted EXAFS signals, $k^2\chi(k)$, were obtained using the Athena software from the Demeter package.[57] The FT curves of the $k^2\chi(k)$ signals were obtained for the $2.8 \leq k \leq 15$ Å^{-1} range, using a sinus window. The EXAFS structural analysis was performed using theoretical phases and amplitudes calculated by the FEFF-6 code,[58] and fits to the experimental data were carried out in R-space with the Artemis program of the Demeter package.[57] ^{1}H and ^{13}C{^{1}H} NMR spectra were recorded on a Bruker Advance 300 (300.1276 MHz and 75.4792 MHz) at room temperature in $CDCl_3$ or acetone-d_6. NMR chemical shifts are reported in ppm relative to tetramethylsilane and referenced to partially deuterated solvent resonances. Coupling constants (*J*) are given in Hertz. NMR assignments are based on homo- and heteronuclear shift correlation spectroscopy. The adopted atom numbering in the cyclometalated compounds starts at the metal-bound carbon (C1), circles toward the nitrogen-bound carbon (C2), and finishes at C6, the carbon ortho to the metal-bound carbon. Electrospray mass spectra (ESI-MS) were recorded on a Bruker Esquire 3000+ spectrometer using sodium formiate as reference.

Single crystals of [Cp*RhI(C,C')-Triaz] (**1**) and [Cp*RhI(C,C')-Im] (**2**)[59] for the X-ray diffraction studies were grown by slow diffusion of n-hexane into a chloroform (**1**) or dichloromethane (**2**) solution of the complex. X-ray diffraction data were collected at 100(2) K on the diffractometers Bruker Bruker APEX DUO CCD (**1**) and SMART APEX CCD (**2**) with graphite-monochromated Mo−Kα radiation (λ = 0.71073 Å) using ω rotations. Intensities were integrated and corrected for absorption effects with SAINT–PLUS[60] and SADABS[61] programs, both included in the APEX2 package. The structures were solved by the Patterson method with SHELXS-97[62] and refined by full matrix least-squares on F^2 with SHELXL-2014,[63] under WinGX.[64]

Crystal data and structure refinement for 1. $C_{25}H_{27}IN_3Rh{\cdot}CHCl_3$, M = 718.67 g mol^{-1}, monoclinic, $P2_1/c$, a = 17.6520(18) Å, b = 12.0217(12) Å, c = 14.0368(14) Å, β = 113.1940(10)°, V = 2738.0(5) Å^3, Z = 4, D_{calc} = 1.743 g cm^{-3}, μ = 2.064 mm^{-1}, F(000) = 1416, prism, orange, 0.180 x 0.120 x 0.030 mm^3, $\theta_{min}/\theta_{max}$ 2.108/26.372°, index ranges: $-22 \leq h \leq 22$, $-15 \leq k \leq 15$, $-17 \leq l \leq 17$,

reflections collected/independent 27926/5598 [R(int) = 0.0821], data/restraints/parameters 5598/0/313, GOF = 1.065, R_1 = 0.0554 [$I>2\sigma(I)$], wR_2 = 0.1110 (all data), largest diff. peak/hole 1.256/–1.225 e·Å^{-3}. CCDC deposit number 1982114.

Crystal data and structure refinement for 2. $C_{20}H_{24}IN_2Rh$, M = 522.22 g mol^{-1}, monoclinic, $P2_1/c$, a = 14.0181(11) Å, b = 8.4600(7) Å, c = 16.4369(13) Å, β = 102.7530(10)°, V = 1901.2(3) Å^3, Z = 4, D_{calc} = 1.824 g cm^{-3}, μ = 2.526 mm^{-1}, F(000) = 1024, prism, orange, 0.170 x 0.120 x 0.020 mm^3, $\theta_{min}/\theta_{max}$ 1.489/27.097°, index ranges $-17\leq h\leq 17$, $-10\leq k\leq 10$, $-21\leq l\leq 20$, reflections collected/independent 22270/4189 [R(int) = 0.0457], data/restraints/parameters 4189/0/223, GOF = 1.018, R_1 = 0.0251[$I>2\sigma(I)$], wR_2 = 0.0522 (all data), largest diff. peak/hole 0.689/–0.514 e Å^{-3}. CCDC deposit number 1982113.

Synthesis of [Cp*RhI(C,C')-Triaz] (1). 1,4-Diphenyl-3-methyl-1,2,3-triazolium iodide (100 mg, 0.270 mmol), $[Cp^*RhCl_2]_2$ (83.4 mg, 0.135 mmol) and NaO*t*Bu (51.9 mg, 0.540 mmol) were reacted in THF (25 mL) at room temperature for 12 hours. After that time, the solution was filtered and then evaporated to dryness under vacuum. The organometallic compound was extracted with CH_2Cl_2 (15 mL) and the resulting dark orange solution was filtered and concentrated to *ca.* 2 mL under reduced pressure. Slow addition of pentane (12 mL) afforded an orange solid which was separated by decantation, washed with pentane (2 x 3 mL) and dried in vacuum. Recrystallization from dichloromethane/pentane gave the compound as a microcrystalline orange solid. Yield: 60.5 mg, 0.101 mmol, 73%. ^{1}H NMR (300 MHz, 298K, $CDCl_3$): δ 7.92 (d, 2H, $J_{H\text{-}H}$ = 8.1, H_o Ph), 7.82 (d, 1H, $J_{H\text{-}H}$ = 7.4, H^6 NPh), 7.64–7.52 (m, 5H, H^3 NPh, and H_m, H_p Ph), 7.15 (t, 1H, $J_{H\text{-}H}$ = 7.3, H^5 NPh), 7.05 (t, 1H, $J_{H\text{-}H}$ = 7.3, H^4 NPh), 4.12 (s, 3H, NCH_3), 1.55 (s, 15H, CH_3 Cp*). ^{13}C{^{1}H} NMR (75 MHz, 298K, $CDCl_3$) δ: 165.9 (d, $J_{C\text{-}Rh}$ = 55.5, C_{Triaz}), 159.7 (d, $J_{C\text{-}Rh}$ = 35.8, C^1 NPh), 145.1 (d, $J_{C\text{-}Rh}$ = 3.4, C^2 NPh), 144.9 ($C_{TriazPh}$), 140.2 (C^6 NPh), 131.0 (C_o, Ph), 129.8 (C_p, Ph), 129.0 (C_m, Ph), 128.2 (C_{ipso} Ph), 127.9 (C^5, NPh), 122.5 (C^4 NPh), 113.9 (C^3 NPh), 97.5 (d, $J_{C\text{-}Rh}$ = 4.9, C Cp*), 37.3 (NCH_3), 10.2, (CH_3 Cp*). Anal. Calc. for $C_{25}H_{27}N_3RhI$: C, 50.10; H, 4.54; N, 7.01. Found C,

50.20; H, 4.73; N, 7.20. HRMS (ESI+, CH_3CN, m/z): Calc. for $C_{25}H_{27}N_3RhI$: 599.3129, $[M]^+$. Found for $C_{25}H_{27}N_3Rh$: 472.1247, $[M\text{-}I]^+$. Found for $C_{15}H_{13}N_3$: 236.1172, $[Triaz]^+$.

Synthesis of [Cp*RhI(C,C')-Im] (2). 1-phenyl-3-methyl-1,3-imidazolium iodide (100 mg, 0.350 mmol), $[Cp^*RhCl_2]_2$ (108 mg, 0.175 mmol) and NaO*t*Bu (67.3 mg, 0.700 mmol) were reacted in a mixture of THF/MeOH (1:1, 25 mL) at room temperature for 12 hours. After that time, the solution was brought to dryness under vacuum and the resulting solid extracted with CH_2Cl_2 (2 x 15 mL). The resulting brown solution was filtered and concentrated to *ca.* 2 mL under reduced pressure. Slow addition of pentane (8 ml) gave a microcrystalline orange solid which was separated by decantation, washed with pentane (2 x 3 mL) and dried in vacuum. Yield: 84.3 mg, 0.148 mmol, 85%. ^1H NMR (300 MHz, 298K, $CDCl_3$): δ 7.69 (dd, 1H, $J_{H\text{-}H}$ = 7.3, 1.3, H^6 Ph), 7.34 (d, 1H, $J_{H\text{-}H}$ = 2.1, CH, Im), 7.13 (dd, $J_{H\text{-}H}$ = 7.3, 1.3, H^3 Ph), 6.97 (d, 1H, $J_{H\text{-}H}$ = 2.1, CH Im), 6.96-6.87(m, 2H, H^5, H^4 Ph), 3.87 (s, 3H, NCH_3), 1.91 (s, 15H, CH_3, Cp*). HRMS (ESI+, CH_3CN, m/z): Calc. for $C_{20}H_{24}N_2RhI$: 522.23, $[M]^+$. Found for $C_{20}H_{24}N_2Rh$: 395.1018, $[M\text{-}I]^+$.

Synthesis of TRGO-Triaz-Rh(III). TRGO-Triaz (60 mg) was dispersed in anhydrous THF (20 mL) in an ultrasonic bath for 30 min. Then, $[Cp^*RhCl_2]_2$ (25 mg, 0.040 mmol) and NaO*t*-Bu (15.36 mg, 0.16 mmol) were sequentially added and the suspension stirred at room temperature for 24 hours. The black solid was washed with MeOH (2 x 15 mL), THF (2 x 10 mL) and Et_2O (1 x 5 mL), with the help of an ultrasonic bath/centrifuge, and dried under vacuum.

TRGO-Triaz treatments: *a)* **TRGO-Triaz** (51.5 mg) was dispersed in anhydrous THF (10 mL) in an ultrasonic bath for 30 min. Then, NaO*t*-Bu (20.34 mg, 0.218 mmol) was added and the suspension stirred at room temperature for 12 hours. The black solid was filtered, washed with MeOH (3 x 7 mL) and Et_2O (1 x 5 ml), with the help of an ultrasonic bath/centrifuge, and dried under vacuum to afford the material **TRGO-Triaz'**. *b)* **TRGO-Triaz** (40 mg) was dispersed in a mixture of *t*-BuOH/H_2O (1:1, 10 mL) in an ultrasonic bath for 30 min. The suspension was stirred at room temperature for 12 hours, washed with MeOH (3 x 7 mL) and Et_2O (1 x 5 ml), with the

help of an ultrasonic bath/centrifuge, and dried under vacuum to afford the material **TRGO-Triaz''**.

General procedure for catalytic alkyne hydrosilylation reactions. Hydrosilylation catalytic tests were carried out in NMR tubes, under an argon atmosphere, in $CDCl_3$ or acetone-d_6. In a typical procedure, a NMR tube was charged under argon with the catalyst ($1x10^{-3}$ mmol, 1 mol %), deuterated solvent (0.5 mL), the corresponding alkyne (0.1 mmol), hydrosilane (0.1 mmol) and anisole (0.01 mmol) as internal standard. The solution was kept at room temperature or in a thermostated bath at 60 °C and monitored by ^{1}H NMR spectroscopy. The weight of the supported catalysts used in each experiment was calculated according to ICP measurements assuming that all the rhodium in the hybrid materials corresponds to active catalyst sites.

The vinylsilane reaction products derived from 1-alkynes were unambiguously characterized on the basis of the coupling patterns and constants of vinylic protons in the ^{1}H NMR spectra and subsequent comparison to literature values.[65] Values for *J* ranged from 17 to 19 Hz for β-(*E*), 13 to 16 Hz for β-(*Z*), and 1 to 3 Hz for α-vinylsilanes.

The recycling of the heterogeneous catalyst was carried out by evaporating the deuterated solvent under vacuum. The residue was washed with hexane (3 x 1 mL) using the centrifuge to remove the organic products and dried in vacuum. Then, another load of reactants and deuterated solvent were added in order to perform a new catalytic cycle under the same experimental conditions.

Synthesis of (*Z*)-dimethyl(oct-1-en-1-yl)(phenyl)silane. A Schlenk tube with a screw cap was charged with catalyst **1** (9.5 mg, 0.0158 mmol), acetone (5 mL), oct-1-yne (1.58 mmol, 241 μL) and $HSiMe_2Ph$ (1.58 mmol, 248 μL). The solution was stirred at room temperature for 30 min until complete consumption of the reactants (NMR) and then a new load of reactants was added. After three consecutive catalytic cycles, the yellow solution was passed through a silica gel column to

give (*Z*)-dimethyl(oct-1-en-1-yl)(phenyl)silane as a colourless liquid (1.13 g, 97%) with only trace amounts of the β-(*E*) vinylisomer after elimination of the solvent.

Computational Details. DFT calculations were performed with the Gaussian09 suite, D.01revision.[66] We selected the B3LYP exchange-correlation functional,[67] with D3BJ dispersion corrections[68] and the "ultrafine" grid. Geometry optimizations were carried out using the df2-SVP basis set, with further energy refinements by means of single point calculations with def2-TZVP.[69] We also applied a PCM implicit model for the solvent (acetone), which we included in both gradients and energy calculations.[70] The nature of the stationary points has been confirmed by analytical frequency analysis. Moreover, we removed the translational entropy contribution to the Gibbs energy as by Morokuma and co-workers.[71] The motivation for the method selection lies on the basis of our previous studies on hydrosilylation reactions catalyzed by Rh- and Ir-based complexes, in which the aforementioned methodology has demonstrated to perform well and provide results in agreement with experimental observations.[37,72] Structure graphical representations were made by means of CylView software.[73]

ASSOCIATED CONTENT

Supporting information

Synthesis of **TRGO-Triaz**, TG, Raman, XPS and STEM-EDX characterization of TRGO-based materials, detailed XAS analysis of rhodium complexes, NMR analysis and reaction profiles for selected hydrosilylation reactions and DFT energetic data and optimized coordenates for catalytic intermediates and transition states is available free of charge via the Internet at http://pubs.acs.org.

AUTHOR INFORMATION

Corresponding Author

M. Victoria Jiménez: vjimenez@unizar.es, tlf: +34 876553794

Jesús J. Pérez-Torrente: perez@unizar.es, tlf: +34 976762025

ORCID

Beatriz Sánchez-Page: 0000-0002-2449-7459

Julen Munarriz: 0000-0001-6089-6126

M. Victoria Jiménez: 0000-0002-0545-9107

Jesús J. Pérez-Torrente: 0000-0002-3327-0918

Javier Blasco: 0000-0002-9706-3272

Gloria Subias: 0000-0002-9029-1977

Vincenzo Passarelli: 0000-0002-1735-6439

Patricia Álvarez: 0000-0001-9676-0546

Author Contributions

The manuscript was written through contributions of all authors. All authors have given approval to the final version of the manuscript.

Notes

The authors declare no competing financial interest.

ACKNOWLEDGEMENTS

The authors express their appreciation for the financial support from MICINN/FEDER, projects PID2019-103965GB-100, CTQ2016-75884-P and RTI2018-098537-B-C22, DGA/FEDER 2014-2020 "*Building Europe from Aragón*" (groups E42_20R and E12_20R) and Principado de Asturias/FEDER (IDI/2018/000121). The authors also acknowledge ALBA synchrotron for granting beamtime and the collaboration of the CLAESS beamline staff.

REFERENCES

(1) Lanzafame, P.; Perathoner, S.; Centi, G.; Gross. S; Hensen, E. J. M. Grand challenges for catalysis in the Science and Technology Roadmap on Catalysis for Europe: moving ahead for a sustainable future. *Catal. Sci. Technol.* **2017**, *7*, 5182–5194.

(2) Somfai, P; Seashore-Ludlow, B. Organosilicon reagent: vinyl-, alkynyl-, and arylsilanes, *Comprehensive Organic Synthesis*, Springer, Amsterdam, Netherlands, 2014.

(3) Komiyama, T.; Minami, Y.; Hiyama, T. Recent Advances in Transition-Metal-Catalyzed Synthetic Transformations of Organosilicon Reagents. *ACS Catal.* **2017**, *7*, 631–651.

(4) Pouget, E.; Tonnar, J.; Lucas, P.; Desmazes, P. L.; Ganachaud, F.; Boutevin, B. Well-Architectured Poly(dimethylsiloxane)-Containing Copolymers Obtained by Radical Chemistry. *Chem. Rev.* **2010**, *110*, 1233–1277.

(5) Pérez-Torrente, J. J.; Nguyen, D. H.; Jiménez, M. V.; Modrego, F. J.; Puerta-Oteo, R.; Gómez-Bautista, D.; Iglesias, M.; Oro, L. A. Hydrosilylation of Terminal Alkynes Catalyzed by a ONO-Pincer Iridium(III) Hydride Compound: Mechanistic Insights into the Hydrosilylation and Dehydrogenative Silylation Catalysis. *Organometallics* **2016**, *35*, 2410–2422.

(6) For examples of selective β-(*E*)-alkenylsilane formation, see: a) Dierick, S.; Vercruysse, E.; Berthon-Gelloz, G.; Markó, I. E. User-Friendly Platinum Catalysts for the Highly Stereoselective Hydrosilylation of Alkynes and Alkenes. *Chem. Eur. J.* **2015**, *21*, 17073−17078. b) Cano, R.; Yus, M.; Ramón, D. J. Impregnated platinum on magnetite as an efficient, fast, and recyclable catalyst for the hydrosilylation of alkynes. *ACS Catal.* **2012**, *2*, 1070–1078. c) Berthon-Gelloz, G.; Schumers, J. -M.; de Bo, G.; Markó, I. E. Highly β-(*E*)-Selective Hydrosilylation of Terminal and Internal Alkynes Catalyzed by a (IPr)Pt(diene) Complex. *J. Org. Chem.* **2008**, *73*, 4190–4197. d) Takeuchi, R.; Nitta, S.; Watanabe, D. A Selective Synthesis of (*E*)-Vinylsilanes by Cationic Rhodium Complex-Catalyzed Hydrosilylation of 1-Alkynes and Tandem Hydrosilylation/Isomerization Reaction of Propargylic Alcohols to β-Silyl Ketones. *J. Org. Chem.* **1995**, *60*, 3045–3051.

(7) For examples of selective α-alkenylsilane formation, see: a) Xie, X.; Zhang, X.; Gao, W.; Meng, C.; Wang, X.; Ding, S. Iridium-catalyzed Markovnikov hydrosilylation of terminal alkynes achieved by using a trimethylsilyl-protected trihydroxysilane. *Commun. Chem.* **2019**, *2*, 101. b) Wu, G.; Chakraborty, U.; von Wangelin, A. J. Regiocontrol in the cobalt catalyzed hydrosilylation of alkynes. *Chem. Commun*. **2018**, *54*, 12322–12325. c) Guo, J.; Lu, Z. Highly chemo-, regio-, and stereoselective cobalt-catalyzed Markovnikov hydrosilylation of alkynes.

Angew. Chem. Int. Ed. **2016**, *55*, 10835–10838. d) Iglesias, M.; Aliaga-Lavrijsen, M.; Sanz Miguel, P. J.; Fernández-Álvarez, F. J.; Pérez-Torrente, J. J.; Oro, L. A. Preferential α-Hydrosilylation of Terminal Alkynes by Bis-N-Heterocyclic Carbene Rhodium(III) Catalysts. *Adv. Synth. Catal.* **2015**, *357*, 350–354. b) Trost, B. M.; Ball, Z. T. Alkyne Hydrosilylation Catalyzed by a Cationic Ruthenium Complex: Efficient and General Trans Addition. *J. Am. Chem. Soc.* **2005**, *127*, 17644–17655.

(8) For examples of selective β-(*Z*)-alkenylsilane formation, see: a) Mutoh, Y.; Mohara, Y.; Saito, S. (*Z*)-Selective Hydrosilylation of Terminal Alkynes with $HSiMe(OSiMe_3)_2$ Catalyzed by a Ruthenium Complex Containing an N-Heterocyclic Carbene. *Org. Lett.* **2017**, *19*, 5204–5207. b) Martín, M.; Sola, E.; Lahoz, F. J.; Oro, L. A. Trans Additions of Silanes to 1-Alkynes Catalyzed by Ruthenium Complexes: Role of in Situ Formed Polynuclear Aggregates. *Organometallics* **2002**, *21*, 4027–4029.

(9) a) Gao, R.; Pahls, D. R.; Cundari, T. R.; Yi, C. S. Experimental and Computational Studies of the Ruthenium Catalyzed Hydrosilylation of Alkynes: Mechanistic Insights into the Regio- and Stereoselective Formation of Vinylsilanes. *Organometallics* **2014**, *33*, 6937−6944. b) Jun, C.-H.; Crabtree, R. H. Dehydrogenative Silation, Isomerization and the Control of Syn- *vs*. Anti-addition in the Hydrosilation of Alkynes. *J. Organomet. Chem.* **1993**, *447*, 177−187.

(10) Zhao, X.; Yang, D.; Zhang, Y.; Wang, B.; Qu, J. Highly β(*Z*)-Selective Hydrosilylation of Terminal Alkynes Catalyzed by Thiolate-Bridged Dirhodium Complexes. *Org. Lett.* **2018**, *20*, 5357−5361.

(11) a) Corre, Y.; Werlé, C.; Brelot-Karmazin, L.; Djukic, J.-P.; Agbossou-Niedercorn, F.; Michon, C. Regioselective hydrosilylation of terminal alkynes using pentamethylcyclopentadienyl iridium(III) metallacycle catalysts. *J. Mol. Catal. A-Chem.* **2016**, *423*, 256–263. b) Iglesias, M.; Pérez-Nicolás, M.; Sanz Miguel, P. J.; Polo, V.; Fernández-Alvarez, F. J.; Pérez-Torrente, J. J.; Oro, L. A. A synthon for a 14-electron Ir(III) species: catalyst for highly selective β-(*Z*) hydrosilylation of terminal alkynes. *Chem. Commun.* **2012**, *48*, 9480–9482. c) Sridevi, V. S.; Fan, W. Y.; Leong, W. K. Stereoselective Hydrosilylation of Terminal Alkynes Catalyzed by $[Cp^*IrCl_2]_2$: A Computational and Experimental Study. *Organometallics* **2007**, *26*, 1157–1160.

(12) a) Conifer, C.; Gunanathan, C.; Rinesch, T.; Hölscher, M.; Leitner, W. Solvent-Free Hydrosilylation of Terminal Alkynes by Reaction with a Nonclassical Ruthenium Hydride Pincer Complex. *Eur. J. Inorg. Chem.* **2015**, 333–339. b) Na, Y.; Chang, S. Highly Stereoselective and Efficient Hydrosilylation of Terminal Alkynes Catalyzed by $[RuCl_2(p\text{-cymene})]_2$. *Org. Lett.* **2000**, *2*, 1887−1889.

(13) a) Chen, J.; Guo, J.; Lu, Z. Recent Advances in Hydrometallation of Alkenes and Alkynes via the First Row Transition Metal Catalysis. *Chin. J. Chem.* **2018**, *36*, 1075−1109. b) Du, X.; Hou, W.; Zhang, Y.; Huang, Z. Pincer Cobalt Complex-Catalyzed *Z*-selective Hydrosilylation of Terminal Alkynes. *Org. Chem. Front.* **2017**, *4*, 1517−1521. c) Teo, W. J.; Wang, C.; Tan, Y. W.; Ge, S. Cobalt-Catalyzed *Z*-Selective Hydrosilylation of Terminal Alkynes. *Angew. Chem. Int. Ed*. **2017**, 56, 4328−4332. d) Sun, J.; Deng, L. Cobalt Complex-Catalyzed Hydrosilylation of Alkenes and Alkynes. *ACS Catal.* **2016**, *6*, 290−300.

(14) a) Challinor, A. J.; Calin, M.; Nichol, G. S.; Carter, N. B.; Thomas, S. P. Amine-Activated Iron Catalysis: Air- and Moisture-Stable Alkene and Alkyne Hydrofunctionalization. *Adv. Synth. Catal.* **2016**, *358*, 2404–2409. b) Greenhalgh, M. D.; Frank, D. J.; Thomas, S. P. Iron-Catalysed Chemo-, Regio-, and Stereoselective Hydrosilylation of Alkenes and Alkynes using a Bench-Stable Iron(II) Pre-Catalyst. *Adv. Synth. Catal.* **2014**, *356*, 584–590.

(15) Liang, H.; Ji, Y.-X.; Wang, R.-H.; Zhang, Z.-H.; Zhang, B. Visible-Light-Initiated Manganese-Catalyzed *E*-Selective Hydrosilylation and Hydrogermylation of Alkynes. *Org. Lett.* **2019**, *21*, 2750−2754.

(16) Peris, E. Smart N-Heterocyclic Carbene Ligands in Catalysis. *Chem. Rev.* **2018**, *118*, 19, 9988−10031.

(17) a) Tyagi, A.; Yadav, S.; Daw, P.; Ravi, C.; Bera, J. K. A Rh(I) complex with an annulated N-heterocyclic carbene ligand for *E*-selective alkyne hydrosilylation. *Polyhedron* **2019**, *172*, 167–174. b) Morales-Cerón, J. P.; Lara, P.; López-Serrano, J.; Santos, L. L.; Salazar, V.; Álvarez, E.; Suárez, A. Rhodium(I) Complexes with Ligands Based on N-Heterocyclic Carbene and Hemilabile Pyridine Donors as Highly E Stereoselective Alkyne Hydrosilylation Catalysts. *Organometallics* **2017**, *36*, 2460−2469. c) Jiménez, M. V.; Pérez-Torrente, J. J.; Bartolomé, M. I.; Gierz, V.; Lahoz, F. J.; Oro, L. A. Rhodium(I) Complexes with Hemilabile N-Heterocyclic Carbenes: Efficient Alkyne Hydrosilylation Catalysts. *Organometallics* **2008**, *27*, 224−234.

(18) a) Puerta-Oteo, R.; Munarriz, J.; Polo, V.; Jiménez, M. V.; Pérez-Torrente, J. J. Carboxylate-Assisted β-(Z) Stereoselective Hydrosilylation of Terminal Alkynes Catalyzed by a Zwitterionic Bis-NHC Rhodium(III) Complex. *ACS Catal.* **2020**, *10*, 7367–7380. b) Iglesias, M.; Sanz Miguel, P. J.; Polo, V.; Fernández-Alvarez, F. J.; Pérez-Torrente, J. J.; Oro, L. A. An Alternative Mechanistic Paradigm for the β-Z Hydrosilylation of Terminal Alkynes: The Role of Acetone as a Silane Shuttle. *Chem. Eur. J.* **2013**, *19*, 17559–17566.

(19) Marichev, K. O.; Patil, S. A.; Bugarin, A. Recent advances in the synthesis, structural diversity, and applications of mesoionic 1,2,3-triazol-5-ylidene metal complexes. *Tetrahedron* **2018**, *74*, 2523−2546.

(20) Crabtree, R. H. Abnormal, Mesoionic and Remote N-H heterocyclic Carbene Complexes. *Coord. Chem. Rev.* **2013**, *257*, 755−766.

(21) See for example: a) Vivancos, A.; Segarra, C.; Albrecht, M. Mesoionic and Related Less Heteroatom-Stabilized N-Heterocyclic Carbene Complexes: Synthesis, Catalysis, and Other Applications. *Chem. Rev.* **2018**, *118*, 9493−9586. b) Mazloomi, Z.; Pretorius, R.; Pàmies, O.; Albrecht, M.; Diéguez, M. Triazolylidene Iridium Complexes for Highly Efficient and Versatile Transfer Hydrogenation of C=O, C=N, and C=C Bonds and for Acceptorless Alcohol Oxidation. *Inorg. Chem.* **2017**, *56*, 11282−11298. c) Wei, Y.; Liu, S.-X.; Mueller-Bunz, H.; Albrecht, M. Synthesis of Triazolylidene Nickel Complexes and Their Catalytic Application in Selective Aldehyde Hydrosilylation. *ACS Catal.* **2016**, *6*, 8192−8200.

(22) Sánchez-Page, B.; Jiménez, M. V.; Pérez-Torrente, J. J.; Passarelli, V.; Blasco, J.; Subias, G; Granda, M.; Álvarez, P. Hybrid Catalysts Comprised of Graphene Modified with Rhodium-Based N-Heterocyclic Carbenes for Alkyne Hydrosilylation. *ACS Appl. Nano Mater.* **2020**, *3*, 1640−1655.

(23) Wang, W.; Cui, L.; Sun, P.; Shi, L.; Yue, C.; Li, F. Reusable N-Heterocyclic Carbene Complex Catalysts and Beyond: A Perspective on Recycling Strategies. *Chem. Rev.* **2018**, *118*, 9843−9929.

(24) a) Lázaro, G.; Fernández-Alvarez, F. J.; Iglesias, M.; Horna, C.; Vispe, E.; Sancho, R.; Lahoz, F. J.; Iglesias, M.; Perez-Torrente, J. J.; Oro, L. A. Heterogeneous Catalysts Based on Supported Rh-NHC Complexes: Synthesis of High Molecular Weight Poly(silylether)s by Catalytic Hydrosilylation. *Catal. Sci. Technol.* **2014**, *4*, 62−70. b) Jankowska-Wajda, M.; Bartlewicz, O.; Szpecht, A.; Zajac, A.; Smiglak, M.; Maciejewski, H. Platinum and Rhodium Complexes Ligated by Imidazolium-Substituted Phosphine as Efficient and Recyclable Catalysts for Hydrosilylation. *RSC Adv.* **2019**, *9*, 29396−29404.

(25) a) Binding, S. C.; Pernik, I.; Gonçales, V. R.; Wong, C. M.; Webster, R. F.; Cheong, S.; Tilley, R. D.; Garcia-Bennett, A. E.; Gooding, J. J.; Messerle, B. A. Simultaneous Functionalization of Carbon Surfaces with Rhodium and Iridium Organometallic Complexes: Hybrid Bimetallic Catalysts for Hydroamination. *Organometallics* **2019**, *38*, 780−787. b) Wong, C. M.; Walker, D. B.; Soeriyadi, A. H.; Gooding, J. J.; Messerle, B. A. A Versatile Method for the Preparation of Carbon–Rhodium Hybrid Catalysts on Graphene and Carbon Black. *Chem. Sci.* **2016**, *7*, 1996–2004.

(26) Ruiz-Botella, S.; Peris, E. Immobilization of Pyrene-Adorned N-Heterocyclic Carbene Complexes of Rhodium(I) on Reduced Graphene Oxide and Study of their Catalytic Activity. *ChemCatChem* **2018**, *10*, 1874–1881.

(27) Ríos, P.; Fouilloux, H.; Díez, J.; Vidossich, P.; Lledós, A.; Conejero, S. σ-Silane Platinum(II) Complexes as Intermediates in C-Si Bond-Coupling Processes. *Chem. Eur. J.* **2019**, *25*, 11346–11355.

(28) a) Pannetier, N.; Sortais J.-B.; Issenhuth, J.-T.; Barloy, L.; Sirlin, C.; Holuigue, A.; Lefort, L.; Panella, L.; de Vries J. G.; Pfeffer, M. Cyclometalated Complexes of Ruthenium, Rhodium and Iridium as Catalysts for Transfer Hydrogenation of Ketones and Imines. *Adv. Synth. Catal*. **2011**, *353*, 2844–2852. b) Espada, M. F.; Esqueda, A. C.; Campos, J.; Rubio, M.; López-Serrano, J.; Álvarez, E.; Maya, C.; Carmona, E. Cationic (η^5-C_5Me_4R)Rh^{III} Complexes with Metalated Aryl Phosphines Featuring η^4-Phosphorus plus Pseudo-Allylic Coordination. *Organometallics* **2018**, *37*, 11−21.

(29) Ghatak, K.; Mane, M.; Vanka, K. Metal or Nonmetal Cooperation with a Phenyl Group: Route to Catalysis? A Computational Investigation. *ACS Catal.* **2013**, *3*, 920−927.

(30) a) Jongbloed, L. S.; de Bruin, B.; Reek, J. N. H.; Lutz, M.; van der Vlugt, J. I. Reversible cyclometalation at Rh^I as a motif for metal–ligand bifunctional bond activation and base-free formic acid dehydrogenation. *Catal. Sci. Technol.* **2016**, *6*, 1320–1327. b) Bhattacharya, P.; Krause, J. A.; Guan, H. Mechanistic Studies of Ammonia Borane Dehydrogenation Catalyzed by Iron Pincer Complexes. *J. Am. Chem. Soc.* **2014**, *136*, 11153–11161.

(31) a) Choi. G.; Tsurugi, H.; Mashima, K. Hemilabile N-Xylyl-N′-methylperimidine Carbene Iridium Complexes as Catalysts for C−H Activation and Dehydrogenative Silylation: Dual Role of N-Xylyl Moiety for ortho-C−H Bond Activation and Reductive Bond Cleavage. *J. Am. Chem. Soc*. **2013**, *135*, 13149−13161. b) Ghoochany, L. T.; Kerner, C.; Farsadpour, S.; Menges, F.; Sun, Y.; Niedner-Schatteburg, G.; Thiel, W. R. C–H Activation at a Ruthenium(II) Complex–The Key Step for a Base-Free Catalytic Transfer Hydrogenation? *Eur. J. Inorg. Chem*. **2013**, 4305–4317.

(32) Donnelly, K. F.; Lalrempuia, R.; Müller-Buz, H.; Albrecht, M. Regioselective Electrophilic C−H Bond Activation in Triazolylidene Metal Complexes Containing a N-Bound Phenyl Substituent. *Organometallics* **2012**, *31*, 8414−8419.

(33) Azpíroz, R.; Rubio-Pérez, L.; Di Giuseppe, A.; Passarelli, V.; Lahoz, F. J.; Castarlenas, R.; Pérez-Torrente, J. J.; Oro, L. A., Rhodium(I)-N-Heterocyclic Carbene Catalyst for Selective

Coupling of N-Vinylpyrazoles with Alkynes via C−H Activation. *ACS Catal.* **2014**, *4*, 4244−4253.

(34) a) Ghoraia, D.; Choudhury J. Exploring a unique reactivity of N-heterocyclic carbenes (NHC) in rhodium(III)-catalyzed intermolecular C–H activation/annulation. *Chem. Commun.* **2014**, *50*, 15159−15162; b) Thenarukandiyil, R.; Gupta, S. K.; Choudhury, J. Unraveling the Competition of Two C−H and Two M−C Bonds in Guiding the Mechanism of Rhodium(III)-Catalyzed C−H Activation−Annulation. *ACS Catal.* **2016**, *6*, 5132−5137.

(35) Busetto, L.; Cassani, M. C.; Femoni, C.; Mancinelli, M.; Mazzanti, A.; Mazzoni, R.; Solinas, G. N-Heterocyclic Carbene-Amide Rhodium(I) Complexes: Structures, Dynamics, and Catalysis. *Organometallics* **2011**, *30*, 5258–5272.

(36) Yamashita, H.; Uchimaru, Y. *Chem. Commun*. **1999**, 1763–1764.

(37) Ojeda-Amador, A. I.; Munarriz, J.; Alamán-Valtierra, P.; Polo, V.; Puerta-Oteo, R.; Jiménez, M. V.; Fernández-Álvarez, F. J.; Pérez-Torrente, J. J. Mechanistic Insights on the Functionalization of CO_2 with Amines and Hydrosilanes Catalyzed by a Zwitterionic Iridium Carboxylate-Functionalized Bis-NHC Catalyst. *ChemCatChem* **2019**, *11*, 5524–5535.

(38) Iglesias, M.; Fernández-Álvarez, F. J.; Oro, L. A. Non-classical Hydrosilane Mediated Reductions Promoted by Transition Metal Complexes. *Coord. Chem. Rev.* **2019**, *386*, 240–266.

(39) Pitman, C. L.; Finster, O. N. L.; Miller, A. J. M. Cyclopentadiene-Mediated Hydride Transfer from Rhodium Complexes. *Chem. Commun.* **2016**, *52*, 9105–9108.

(40) Hallam, B. F.; Pauson, P. L. Ferrocene Derivatives. Part III. Cyclopentadienyl Iron Carbonyls. *J. Chem. Soc.* **1956**, 3030–3037.

(41) Perutz, R. N.; Sabo-Etienne, S. The sigma-CAM Mechanism: sigma complexes as the basis of sigma-bond metathesis at late-transition-metal centers. *Angew. Chem. Int. Ed. Engl.* **2007**, *46*, 2578–2592.

(42) Julián, A.; Guzmán, J.; Jaseer, E. A.; Fernández-Alvarez, F. J.; Royo, R.; García-Orduña, P.; Lahoz, F. J.; Oro. L. A. Mechanistic Insights on the Reduction of CO_2 to Silylformates Catalyzed by Ir-NSiN species. *Chem. Eur. J.* **2017**, *23*, 11898–11907.

(43) Chalk, A. J.; Harrod, J. F. Homogeneous Catalysis. II. The Mechanism of the Hydrosilation of Olefins Catalyzed by Group VIII Metal Complexes. *J. Am. Chem. Soc.* **1965**, *87*, 16– 21.

(44) Vásquez-Céspedes, S.; Wang, X.; Glorius, F. Plausible Rh(V) Intermediates in Catalytic C–H Activation Reactions. *ACS Catal.* **2018**, *8*, 242–257.

(45) Frohnapfel, D. S.; Templeton, J. L. Transition metal η^2-vinyl complexes. *Coord. Chem. Rev.* **2000**, *206*, 199–235.

(46) Kozuch, S.; Shaik, S. How to Conceptualize Catalytic Cycles? The Energetic Span Model. *Acc. Chem. Res.* **2011**, *44*, 101–110.

(47) Even though **G** and **TS-DE** are the lowest- and highest-in-energy reaction intermediate and transition state, they are not the couple determining $\Delta G^{\ddagger}$, as when the barrier determining transition state appears before the intermediate, it is necessary to add the cycle ΔG to their energy difference, which in this case would lead to the meaningless value of $\Delta G^{\ddagger}$ = 14.3 – (-23.0) + (-39.2) = -1.9 kcal·mol^{-1} for the first cycle. Since we predict that subsequent catalytic cycles start in **D**', the $\Delta G^{\ddagger}$ value if we consider **G** and **TS-DE** as the TOF-determining TS and intermediate would be $\Delta G^{\ddagger}$ = 14.3 – (-23.0) + (-32.9) = 4.4 kcal·mol^{-1}, which is lower than the actual energy span determined by **G** and **TS-GD** (12.0 kcal·mol^{-1}).

(48) a) Nieto, J.; Jiménez, M. V.; Álvarez, P.; Pérez-Mas, A. M.; González, Z.; Pereira, R.; Sánchez-Page, B.; Pérez-Torrente, J. J.; Blasco, J.; Subías, G.; Blanco, M.; Menéndez, R. Enhanced Chemical and Electrochemical Water Oxidation Catalytic Activity by Hybrid Carbon Nanotube-Based Iridium Catalysts Having Sulfonate-Functionalized NHC ligands. *ACS Appl. Energy Mater*. **2019**, *2*, 3283–3296. b) Blanco, M.; Álvarez, P.; Blanco, C.; Jiménez, M. V.; Pérez-Torrente, J. J.; Oro, L. A.; Blasco, J.; Cuartero, V.; Menéndez, R. Enhancing the Hydrogen Transfer Catalytic Activity of Hybrid Carbon Nanotube-Based NHC-Iridium Catalysts by Increasing the Oxidation Degree of the Nanosupport. *Catal. Sci. Technol.* **2016**, *6*, 5504–5514.

(49) NIST database: NIST X-ray Photoelectron Spectroscopy Database. NIST Standard Reference Database 20, Version 4.1. http://dx.doi.org/10.18434/T4T88K.

(50) Rhodium(I) complexes can promote undesirable polymerization of aryl-substituted alkynes such as phenylacetylene. See, for example: Mori, A.; Takahisa, E.; Yamamura, Y.; Kato, T.; Mudalige, A. P.; Kajiro, H.; Hirabayashi, K.; Nishihara, Y.; Hiyama, T. Stereodivergent Syntheses of (*Z*)- and (*E*)-Alkenylsilanes via Hydrosilylation of Terminal Alkynes Catalyzed by Rhodium(I) Iodide Complexes and Application to Silicon-Containing Polymer Syntheses. *Organometallics* **2004**, *23*, 1755–1765.

(51) Mangione, M. I.; Spanevello, R. A.; Anzardi M. B., Efficient and straightforward click synthesis of structurally related dendritic triazoles. *RSC Adv.* **2017**, *7*, 47681–47688.

(52) Liu, J.; Chen, J.; Zhao, J.; Zhao, J.; Li, L.; Zang, H. A Modified Procedure for the Synthesis of 1-Arylimidazoles. *Synthesis* **2003**, *17*, 2661–2666.

(53) White, C.; Yates, A.; Maitlis, P. M.; Heinekey, D. M. (η^5-Pentamethylcyclopentadienyl)Rhodium and -Iridium Compounds. In *Inorganic Syntheses*; John Wiley & Sons, Inc, 1992; Vol. 29, pp 228−234.

(54) Sherwood, P. M. A. In *Practical Surface Analysis in Auger and X-ray Photoelectron Spectroscopy*; Briggs, D.; Seah, M. P. Eds.; Wiley: New York, 1990, 2nd ed. vol. 1, pp. 657.

(55) Elgrabli, D.; Floriani, M.; Abella-Gallar, S.; Meunier, L.; Gamez, C.; Delalain, P.; Rogerieux, F.; Boczkowski, J.; Lacroix, G. Biodistribution and Clearance of Instilled Carbon Nanotubes in Rat Lung. *Part. Fibre. Toxicol.* **2008**, *5*, 20–33.

(56) Simonelli, L.; Marini, C.; Olszewski, W.; Avila Perez, M.; Ramanan, N.; Guilera, G.; Cuartero, V.; Klementiev, K. CLÆSS: the hard x-ray absorption beamline of the ALBA CELLS synchrotron. *Cogent Physics* **2016**, *3*, 1231987.

(57) Ravel, B.; Newville, M. ATHENA, ARTEMIS, HEPHAESTUS: data analysis for X-ray absorption spectroscopy using IFEFFIT. *J. Synchrotron Radiat.* **2005**, *12*, 537−541.

(58) Rehr, J. J.; Albers, R. C. Theoretical approaches to x-ray absorption fine structure. *Rev. Mod. Phys.* **2000**, *72*, 621−654.

(59) The crystal structure of **2** was previously reported by Choudhury *et al.* (ref. 34). Nonetheless the poor quality of that determination {R1 = 0.1211 [I>2σ(I)], wR2 = 0.4370 (all data)} prompted us to carry out a significantly more accurate determination at 100 K.

(60) SAINT+: Area-Detector Integration Software, version 6.01; Bruker AXS: Madison, WI, 2001.

(61) Sheldrick, G. M. SADABS program; University of Göttingen: Göttingen, Germany, 1999.

(62) Sheldrick, G. M. SHELXS 97, Program for the Solution of Crystal Structure; University of Göttingen: Göttingen, Germany, 1997.

(63) Sheldrick, G. M. Crystal structure refinement with SHELXL. *Acta Crystallogr. Sect. C: Struct. Chem.* **2015**, *71*, 3−8.

(64) Farrugia, L. J. WinGX and ORTEP for Windows: an update. *J. Appl. Crystallogr.* **2012**, *45*, 849−854.

(65) a) Derivatives from n-BuC≡CH: Jun, C. H.; Crabtree, R. H., Dehydrogenative silation, isomerization and the control of syn- vs. anti-addition in the hydrosilation of alkynes. *J. Organomet. Chem.* **1993**, *447*, 177−187. b) Derivates from n-HexC≡CH: Nakamura, S.; Uchiyama, M.; Ohwada, T. Chemoselective Silylzincation of Functionalized Terminal Alkynes Using Dianion-Type Zincate (SiBNOL-Zn-ate): Regiocontrolled Synthesis of Vinylsilanes. *J. Am. Chem. Soc*. **2004**, *126*, 11146−11147. c) Derivates from *t*-BuC≡CH: Andavan, G. T. S.; Bauer, E. B.; Letko, C. S.; Hollis, T. K.; Tham, F. S. Synthesis and

Characterization of a Free Phenylene bis(N-heterocyclic carbene) and its di-Rh Complex: Catalytic Activity of the di-Rh and CCC-NHC Rh Pincer Complexes in Intermolecular Hydrosilylation of Alkynes. *J. Organomet. Chem.* **2005**, *690*, 5938−5947. d) Derivatives from PhC≡CH: Katayama, H.; Taniguchi, K.; Kobayashi, M.; Sagawa, T.; Minami, T.; Ozawa, F. J. Ruthenium-Catalyzed Hydrosilylation of Terminal Alkynes: Stereodivergent Synthesis of (*E*)- and (*Z*)-Alkenylsilanes. *J. Organomet. Chem.* **2002**, *645*, 192−200.

(66) Frisch, M. J.; Trucks, G. W.; Schlegel, H. B.; Scuseria, G. E.; Robb, M. A.; Cheeseman, J. R.; Scalmani, G.; Barone, V.; Mennucci, B.; Petersson, G. A.; Nakatsuji, H.; Caricato, M.; Li, X.; Hratchian, H. P.; Izmaylov, A. F.; Bloino, J.; Zheng, G.; Sonnenberg, J. L.; Hada, M.; Ehara, M.; Toyota, K.; Fukuda, R.; Hasegawa, J.; Ishida, M.; Nakajima, T.; Honda, Y.; Kitao, O.; Nakai, H.; Vreven, T.; Montgomery Jr. J. A.; Peralta, J. E.; Ogliaro, F.; Bearpark, M.; Heyd, J. J.; Brothers, E.; Kudin, K. N.; Staroverov, V. N.; Kobayashi, R.; Normand, J.; Raghavachari, K.; Rendell, A.; Burant, J. C.; Iyengar, S. S.; Tomasi, J.; Cossi, M.; Rega, N.; Millam, J. M.; Klene, M.; Knox, J. E.; Cross, J. B.; Bakken, V.; Adamo, C.; Jaramillo, J.; Gomperts, R.; Stratmann, R. E.; Yazyev, O.; Austin, A. J.; Cammi, R.; Pomelli, C.; Ochterski, J. W.; Martin, R. L.; Morokuma, K.; Zakrzewski, V. G.; Voth, G. A.; Salvador, P.; Dannenberg, J. J.; Dapprich, S.; Daniels, A. D.; Farkas, Ö.; Foresman, J. B.; Ortiz, J. V; Cioslowski, J.; Fox, D. J. Gaussian 09, revision D.01; Gaussian, Inc.; Wallingford CT, 2009.

(67) Becke, A. D. A new mixing of Hartree–Fock and local density-functional theories. *J. Chem. Phys.* **1993**, *98*, 1372–1377.

(68) a) Grimme, S.; Antony, J.; Ehrlich, S.; Krieg, H. A consistent and accurate ab initio parametrization of density functional dispersion correction (DFT-D) for the 94 elements H-Pu. *J. Chem. Phys.* **2010**, *132*, 154104. b) Johnson, E. R. E.; Becke, A. D. A. A post-Hartree–Fock model of intermolecular interactions. *J. Chem. Phys.* **2005**, *123*, 024101.

(69) Weigend, F.; Ahlrichs, R. Balanced basis sets of split valence, triple zeta valence and quadruple zeta valence quality for H to Rn: Design and assessment of accuracy. *Phys. Chem. Chem. Phys.* **2005**, *7*, 3297–3305.

(70) Scalmani, G.; Frisch, M. J. Continuous surface charge polarizable continuum models of solvation. I. General formalism. *J. Chem. Phys.* **2010**, *132*, 114110.

(71) Tanaka, R.; Yamashita, M.; Chung, L. W.; Morokuma, K.; Nozaki, K. Mechanistic Studies on the Reversible Hydrogenation of Carbon Dioxide Catalyzed by an Ir-PNP Complex. *Organometallics* **2011**, *30*, 6742–6750.

(72) Lázaro, G.; Fernández-Álvarez, F. J.; Munárriz, J.; Polo, V.; Iglesias, M.; Pérez-Torrente, J. J.; Oro, L. A. Orthometallation of N-substituents at the NHC ligand of [Rh(Cl)(COD)(NHC)]

complexes: its role in the catalytic hydrosilylation of ketones. *Catal. Sci. Technol.* **2015**, *5*, 1878–1887.

(73) CYLview, 1.0b; Legault, C. Y., Université de Sherbrooke, 2009 (http://www.cylview.org).

For Table of Contents (TOC)